ΕΘΝΙΚΟ ΜΕΤΣΟΒΙΟ ΠΟΛΥΤΕΧΝΕΙΟ
ΣΧΟΛΗ ΗΛΕΚΤΡΟΛΟΓΩΝ ΜΗΧΑΝΙΚΩΝ
ΚΑΙ ΜΗΧΑΝΙΚΩΝ ΥΠΟΛΟΓΙΣΤΩΝ
ΤΟΜΕΑΣ ΣΥΣΤΗΜΑΤΩΝ ΜΕΤΑΔΟΣΗΣ ΠΛΗΡΟΦΟΡΙΑΣ
ΚΑΙ ΤΕΧΝΟΛΟΓΙΑΣ ΥΛΙΚΩΝ

DEUTCHES ZENTRUM FÜR LUFT- UND RAUMFAHRT
ΓΕΡΜΑΝΙΚΟ ΑΕΡΟΔΙΑΣΤΗΜΙΚΟ ΚΕΝΤΡΟ
ΙΝΣΤΙΤΟΥΤΟ ΕΠΙΚΟΙΝΩΝΙΩΝ ΚΑΙ ΠΛΟΗΓΗΣΗΣ
ΤΜΗΜΑ ΨΗΦΙΑΚΩΝ ΔΙΚΤΥΩΝ
ΟΜΑΔΑ ΟΠΤΙΚΩΝ ΕΠΙΚΟΙΝΩΝΙΩΝ

Εφαρμογές επικοινωνιών LASER σε δορυφορικά δίκτυα και στρατοσφαιρικές πλατφόρμες

ΔΙΠΛΩΜΑΤΙΚΗ ΕΡΓΑΣΙΑ

ΣΤΑΘΟΠΟΥΛΟΣ ΦΩΤΙΟΣ

Επιβλέπων: Φίλιππος Κωνσταντίνου
         Καθηγητής Ε.Μ.Π.

Επιβλέπων: Νίκολας Περλό
         διδάκτορας

Oberpfaffenhofen, Φεβρουάριος - Ιούλιος 2007

ΕΘΝΙΚΟ ΜΕΤΣΟΒΙΟ ΠΟΛΥΤΕΧΝΕΙΟ
ΣΧΟΛΗ ΗΛΕΚΤΡΟΛΟΓΩΝ ΜΗΧΑΝΙΚΩΝ
ΚΑΙ ΜΗΧΑΝΙΚΩΝ ΥΠΟΛΟΓΙΣΤΩΝ
ΤΟΜΕΑΣ ΣΥΣΤΗΜΑΤΩΝ ΜΕΤΑΔΟΣΗΣ ΠΛΗΡΟΦΟΡΙΑΣ
ΚΑΙ ΤΕΧΝΟΛΟΓΙΑΣ ΥΛΙΚΩΝ

DEUTCHES ZENTRUM FÜR LUFT- UND RAUMFAHRT
ΓΕΡΜΑΝΙΚΟ ΑΕΡΟΔΙΑΣΤΗΜΙΚΟ ΚΕΝΤΡΟ
ΙΝΣΤΙΤΟΥΤΟ ΕΠΙΚΟΙΝΩΝΙΩΝ ΚΑΙ ΠΛΟΗΓΗΣΗΣ
ΤΜΗΜΑ ΨΗΦΙΑΚΩΝ ΔΙΚΤΥΩΝ
ΟΜΑΔΑ ΟΠΤΙΚΩΝ ΕΠΙΚΟΙΝΩΝΙΩΝ

Εφαρμογές επικοινωνιών LASER σε δορυφορικά δίκτυα και στρατοσφαιρικές πλατφόρμες

ΔΙΠΛΩΜΑΤΙΚΗ ΕΡΓΑΣΙΑ

ΣΤΑΘΟΠΟΥΛΟΣ ΦΩΤΙΟΣ

Επιβλέπων: Φίλιππος Κωνσταντίνου
           Καθηγητής Ε.Μ.Π.

Επιβλέπων: Νίκολας Περλό
           διδάκτορας

Oberpfaffenhofen, Φεβρουάριος - Ιούλιος 2007

ΕΘΝΙΚΟ ΜΕΤΣΟΒΙΟ ΠΟΛΥΤΕΧΝΕΙΟ
ΣΧΟΛΗ ΗΛΕΚΤΡΟΛΟΓΩΝ ΜΗΧΑΝΙΚΩΝ
ΚΑΙ ΜΗΧΑΝΙΚΩΝ ΥΠΟΛΟΓΙΣΤΩΝ
ΤΟΜΕΑΣ ΣΥΣΤΗΜΑΤΩΝ ΜΕΤΑΔΟΣΗΣ ΠΛΗΡΟΦΟΡΙΑΣ
ΚΑΙ ΤΕΧΝΟΛΟΓΙΑΣ ΥΛΙΚΩΝ

DEUTCHES ZENTRUM FÜR LUFT- UND RAUMFAHRT
ΓΕΡΜΑΝΙΚΟ ΑΕΡΟΔΙΑΣΤΗΜΙΚΟ ΚΕΝΤΡΟ
ΙΝΣΤΙΤΟΥΤΟ ΕΠΙΚΟΙΝΩΝΙΩΝ ΚΑΙ ΠΛΟΗΓΗΣΗΣ
ΤΜΗΜΑ ΨΗΦΙΑΚΩΝ ΔΙΚΤΥΩΝ
ΟΜΑΔΑ ΟΠΤΙΚΩΝ ΕΠΙΚΟΙΝΩΝΙΩΝ

Εφαρμογές επικοινωνιών LASER σε δορυφορικά δίκτυα και στρατοσφαιρικές πλατφόρμες

ΔΙΠΛΩΜΑΤΙΚΗ ΕΡΓΑΣΙΑ

ΣΤΑΘΟΠΟΥΛΟΣ ΦΩΤΙΟΣ

Επιβλέπων: Φίλιππος Κωνσταντίνου
Καθηγητής Ε.Μ.Π.

Επιβλέπων: Νίκολας Περλό
Διδάκτορας

Εγκρίθηκε από την τριμελή εξεταστική επιτροπή την 31^{η} Οκτωβρίου 2007

....
Φίλιππος Κωνσταντίνου
Καθηγητής Ε.Μ.Π.

....
Νικόλαος Ουζούνογλου
Καθηγητής Ε.Μ.Π.

....
Χρήστος Καψάλης
Καθηγητής Ε.Μ.Π.

Oberpfaffenhofen, Φεβρουάριος - Ιούλιος 2007

....

Φώτιος Π. Σταθόπουλος

Διπλωματούχος Ηλεκτρολόγος Μηχανικός και Μηχανικός Υπολογιστών Ε.Μ.Π.

Σημείωμα του συγγραφέα

Η διπλωματική εργασία συγγράφηκε την περίοδο Φεβρουαρίου – Ιουλίου 2007 στο Oberpfaffenhofen. Η πρωτότυπη εργασία έχει τίτλο «Impact of Aircraft Boundary Layer Turbulence on Laser Beam Propagation» και είναι γραμμένη στα αγγλικά. Είναι καταχωρημένη στο αρχείο της DLR. Για ακαδημαϊκούς λόγους ο τίτλος μεταφράστηκε ως «Εφαρμογές επικοινωνιών LASER σε δορυφορικά δίκτυα και στρατοσφαιρικές πλατφόρμες». Σε αυτό το σημείο θα ήθελα να ευχαριστήσω την οικογένειά μου για την αμέριστη συμπαράστασή της.

Φώτης Σταθόπουλος

NATIONAL TECHNICAL UNIVERSITY OF ATHENS

SCHOOL OF ELECTRICAL AND COMPUTER ENGINEERING

DIVISION OF TRANSMISSIONS SYSTEMS AND MATERIAL
TECHNOLOGIES

DEUTCHES ZENTRUM FÜR LUFT- UND RAUMFAHRT

GERMAN AEROSPACE CENTER

INSTITUTE OF COMMUNICATION UND NAVIGATION

DEPARTMENT OF DIGITAL NETWORKS

OPTICAL GROUP

Impact of aircraft boundary-layer on laser beam propagation

DIPLOMA THESIS

STATHOPOULOS FOTIOS

supervisor: Constantinou Fillipos
             Professor of NTUA

supervisor: Perlot Nicolas
             PhD

Oberpfaffenhofen, February – July 2007

Acknowledgments

Abstract

The last years is noticed a great progress of the optical communications. One of the latest stages of this research is achieving an optical link with an aircraft. This includes links of aircraft - aircraft, aircraft - satellite and aircraft - earth base.

Having optical links at the aircrafts, we will benefit the advantages of the laser links. They propagate with a high speed, and in very long distances. They have very high data rates, and they are very reliable. This means that optical links can be used for secure information transmission.

In this diploma thesis we find a method to calculate the wavefront distortions of a laser beam which starts or ends to propagate to a flying object (aircraft). So firstly we find the flow field around the object, and then find define the method, that we calculate the distortions.

This is the beginning of the research in this topic. We will start from the simplest cases of the flying object shape and the flow around it. The object is a sphere and is considered as the turret of the antenna. Inside the sphere, there is a concentric circular antenna, creating a flat circular laser beam. Since we know the flow around the sphere, we are able to calculate the properties of the fluid, which is air in our case. After we calculate the aberration of the properties we can calculate the distortions of the wavefront.

The results are valid for every conditions of the sphere. We refer to the size of the sphere (turret), and also to the size of the aperture. They are presented for any elevation angle of the beam, but as the sphere is symmetrical we do not consider the angle of attack. We can see the effect of the speed of the sphere (or of the fluid) at the distortions, and finally we have the case of a sphere in the atmosphere, so we can see the effect of the different altitude. The method for the distortion calculation is a general method, which we can apply in any case. So we present and compare all the different kinds of flow, and not only around a sphere, as well as flow around other shapes. We can observe how the properties value change and how these effect the wavefront distortions.

We succeed to have the first idea of the impact of the flow field around a flying object on a laser beam. We see how the boundary layers are created and how they can affect the beam, and we set the base, for further research on this topic.

Key words

boundary layer, Navier - Stokes equations, Reynolds number, turbulence, laminar flow, potential flow, laser beam propagation, wavefront distortions

Περίληψη

Τα τελευταία χρόνια παρατηρείτε σπουδαία πρόοδος στις ασύρματες οπτικές τηλεπικοινωνίες, χρησιμοποιώντας ακτίνες laser. Ένας από τους τελευταίους στόχους της έρευνας σε αυτόν τον τομέα είναι η επίτευξη οπτικής σύνδεσης αεροσκάφους, είτε με κάποιο άλλο αεροσκάφος, είτε ανάμεσα σε ένα αεροσκάφος και ένα δορυφόρο, είτε ανάμεσα σε ένα αεροσκάφος και μία βάση ελέγχου που βρίσκεται στη γη.

Μέσω της οπτικής σύνδεσης, εκμεταλλευόμαστε όλα τα πλεονεκτήματα των laser. Οι ταχύτητες διάδοσης είναι πολύ υψηλές, ενώ μπορεί να διαδίδεται σε πολύ μεγάλες αποστάσεις. Ο ρυθμός διάδοσης είναι πολύ υψηλός, ενώ οι συνδέσεις είναι πολύ αξιόπιστες. Αυτό σημαίνει πως τέτοιες συνδέσεις είναι ασφαλής, ώστε να χρησιμοποιηθούν για μετάδοση απόρρητων πληροφοριών.

Σε αυτή τη διπλωματική εργασία θα μελετήσουμε την παραμόρφωση της κυματομορφής μιας ακτίνας laser η οποία διαδίδεται από ή προς το αεροσκάφος. Αυτό θα το επιτύχουμε ορίζοντας τη μέθοδο που θα μπορέσουμε να υπολογίσουμε αυτήν την παραμόρφωση. Η τελευταία δημιουργείται από την αλλαγή της ροής του αέρα γύρω από το ιπτάμενο αντικείμενο.

Αυτή τη στιγμή βρισκόμαστε στο αρχικό στάδιο της έρευνας. Θα αρχίσουμε από την απλούστερη περίπτωση ιπτάμενου αντικειμένου, το οποίο είναι η σφαίρα. Θεωρούμε μια ομόκεντρη κυκλική κεραία η οποία διαδίδει έναν επίπεδο κυκλικό παλμό. Γνωρίζοντας την ροή του αέρα γύρω από το αντικείμενο θα μπορέσουμε να ορίσουμε την παραμόρφωση του παλμού. Για να το καταφέρουμε θα πρέπει να υπολογίσουμε τις χαρακτηριστικές ιδιότητες του αέρα (πυκνότητα, πίεση κ.α.), η διακύμανση των οποίων επιφέρει τις αλλαγές στην κυματομορφή.

Τα αποτελέσματα αναφέρονται σε κάθε περίπτωση σφαίρας. Αυτό σημαίνει πως θα ερευνήσουμε τα αποτελέσματα ως προς το μέγεθος της διαμέτρου της σφαίρας αλλά και ως προς την ταχύτητά της. Θα μελετήσουμε την παραμόρφωση ως προς την γωνία διάδοσης της ακτίνας. Φυσικά λόγω της συμμετρίας της σφαίρας δεν θα λάβουμε υπόψιν την γωνία πρόσπτωσης του αντικειμένου ως προς τον άξονα της κίνησης. Θα μελετήσουμε την επίδραση του υψόμετρου, άρα της ατμόσφαιρας, στις ιδιότητες του αέρα και τελικά στον παλμό. Τέλος θα συγκρίνουμε τα αποτελέσματά μας με αυτά ιπταμένων αντικειμένων με διαφορετικό σχημάτων (π.χ. airfoils).

Σε αυτή τη διπλωματική επιτυγχάνουμε να καταλάβουμε την επίπτωση της ροής του αέρα γύρω από ένα ιπτάμενο αντικείμενο, σε μια διαδιδόμενη ακτίνα laser. Έτσι θα καταφέρουμε να δημιουργήσουμε κατάλληλες κεραίες για να επιτύχουμε την προσδοκώμενη επικοινωνία.

Λέξεις κλειδιά

διάδοση ακτινών laser, εξισώσεις Navier – Stokes, παραμόρφωση κυματομορφής, παραμόρφωση κυματομορφής, αριθμός Reynold

Contents

Figures

Tables

page

1

Introduction

1.1 Purpose of the Thesis

The purpose of the thesis is to calculate the laser beam distortions, which are created from the flow of an aircraft. The final goal of the thesis is to achieve an optical link between an aircraft and another aircraft, a satellite or an earth-base.

1.2 Encouragement of the Thesis

Creating an optical link with, we can benefit all the advantages of the laser. As we mentioned in the previous paragraph the goal is to achieve an optical link with an aircraft. In most cases the aircraft will be UAV, which is guided from the earth. The link can be either directly from the earth-base, or through a satellite. Of course we have to take in mind the case that two aircrafts have direct communication.

With an optical link we will have faster, with higher bandwidth and more secured communication, and the control time of the information will reduce. In this way we improve the aircraft communication.

Now we are in the beginning of this research. In December of 2006 was the first successful experiment, of an optical link between an airplane and a satellite. This was the LOLA experiment from EADS - Astrium. Now, after we achieved the link, it is very interesting to simulate and calculate the distortions of the beam, in order to create reliable and useful links.

1.3 Synopsis of the Thesis

The thesis is divided in two parts. In the beginning we have an introduction in the Fluid Dynamics and in the conditions of the air. The second part refers to the method we use to evaluate the wavefront distortions. Firstly we have to describe the kind of flow around the object. Then we present the method. This method can be used for any kind of flow.

Chapter 1: In chapter one, we have an introduction of the thesis. We analyze the purpose of the thesis and present its goals.

Chapter 2: In the second chapter we have an introduction with fluid dynamics. This is the science which deals with the fluids, which is the medium of the propagating beam. We see the different types of flow, the boundary layers and then the Navier-Stokes equations and all the equations that describe the flow we have.

Chapter 3: The third chapter describes the fluid we have, which is the air. We see the influence of the beam wavelength and the air density at the performance of the beam. Then we see how the density changes along the height and how it is related to the other air properties.

Chapter 4: In the forth chapter we develop the method to calculate the distortions. We start from the first case. We consider the turret as a sphere and inside there is a concentric antenna. We calculate the wavefront fluctuations with the mean tilt of the wavefront, with the Zernike polynomials and with the RMS value. The fluctuations are function of the elevation angle of the beam, of the ratio of the aperture and the turret diameters and of the free-stream properties.

Chapter 5: The last chapter is the conclusion of the thesis. There are presented the general results of the thesis, and we refer to the future research on this topic, which will be very interesting.

2

Fluid Dynamics

2.1 Introduction

In the thesis we will research the influence of the medium on a laser beam. The medium is a fluid. So we have to know the performance of the fluid, around the moving object. If we find out which type of flow it is, we can use the equations that are valid for this type of flow, and evaluate the properties of the fluid. In this chapter we will have an introduction in fluid dynamics, which is the science which studies the fluids and the flow inside them.

2.2 Newtonian Fluids

A Newtonian fluid is a fluid which has continues flow, independent from the forces acting on it. The stress and the rate of strain curve of the fluid are linear. A fluid is described Newtonian or non-Newtonian from the viscosity. For Newtonian fluids we have the following equation:

$$\tau = \mu \frac{du}{dx}, \tag{2.1}$$

where τ is the shear stress exerted by the fluid, μ is the absolute dynamic fluid viscosity and du/dx is the velocity gradient perpendicular to the direction of shear.

Newtonian fluids have constant viscosity. If the viscosity is very high, the previous equation is not valid, and the fluid is considered as non-Newtonian. In the thesis we consider only Newtonian fluids.

2.3 Navier – Stokes equations

The Navier - Stokes equations describe the flow inside a fluid. They exist since the early 19th century after Claude-Luis Navier and George Gabriel Stokes. Until now they are not well understood, and this is one of the biggest mathematics problems today. These equations are relationships between velocity, pressure, density, temperature and the viscosity. They are extension of the Euler equations, which do

not include the viscosity. There are many forms of these equations, but the most general is the following equation:

$$\rho \frac{DU}{Dt} = -\nabla p + \nabla \cdot T + f , \qquad (2.2)$$

where ρ is the density, ∇p is a pressure gradient, $\nabla \cdot T$ represents the shear forces and f represents all the other forces (ex. gravity).

$\frac{DU}{Dt}$ is the convective derivative:

$$\frac{DU}{Dt} = \frac{\partial U}{\partial t} + (U \cdot \nabla)U ,$$

(2.3)

where t is the time and U is the velocity.

For the velocity we have:

$$\vec{U} = \vec{u} + \vec{v} + \vec{w} \qquad (2.4)$$

2.4 Reynolds number

The Reynolds number is the ratio of inertial forces to viscous forces on the object inside a fluid.

$$Re = \frac{Inertial\ forces}{Viscous\ forces} = \frac{\rho \cdot U^2 / L_c}{\mu \cdot U / L_c^2} = \frac{\rho \cdot U \cdot L_c}{\mu} = \frac{U \cdot L_c}{\nu} , \qquad (2.5)$$

where ρ is the density of the fluid (kg/m^3), U is the fluid velocity (m/s), L_c is a characteristic length (m), μ is the absolute dynamic fluid viscosity (Pa $\times$ s), and ν is the kinematic fluid viscosity (m^2/s), where $\nu = \mu / \rho$.

Reynolds number shows us the amplitude of the effect of each kind of forces at the movement of the fluid. The bigger this number is, the stronger effects are at the fluid properties. The Reynolds number increases as the speed of the object increase, or if the dimensions (the characteristic length) grow. Reynolds number is also depended on the kind of the fluid, and its viscosity (ex. water has 15 times smaller viscosity than the air [1]). This is the value that characterizes a flow in many ways.

2.5 Types of Flow

Since we know the type of the flow, we can find the equations that are valid in this flow, and calculate the unknown properties of the fluid. Then we will be able to find the distortions of the propagating beam inside the fluid. Here are presented some categories of different types of flow.

2.5.1 Laminar or Turbulent Flow

Laminar flow is described from parallel streamlines, with no disruption between them. It complies with linear equations. There is high momentum diffusion, and low momentum convection. The equations of laminar flow are simplifications of the Navier-Stokes equations.

On the other hand there is the turbulent flow, where we have chaotic, stochastic property changes, low momentum diffusion and high momentum convection. It is difficult to set clear layers in turbulent flow, as there is no way to define their borders, because of the random changes. It is believed that the Navier – Stokes equations are valid for turbulent flows, but it is not proved yet.

The value that describes weather a flow is laminar or turbulent is the Reynolds number. The critical number where there is transition from one type to the other depends on the shape of the flying object, its velocity and the angle of attack.

2.5.2 Steady or Unsteady flow

The steady flow is a flow that does not change along the time. This means that if an observer looks at the flow in two different moments he will see the same flow. It can be described from the equation:

$$\partial/\partial t = 0 \qquad\qquad (2.6)$$

After it turns from steady to unsteady, it is still laminar, but when the Reynolds number is so high, it turns from unsteady, laminar, to turbulent (of course it is still unsteady but we neglect to mention).

2.5.3 Compressible or Incompressible Flow

Compressibility is the measure that shows how much is the volume change caused by the pressure. Since the volume varies, we have different density. In other words if the pressure distortions, because of the flight, can bring changes at the density, we have a compressible flow. If the changes at the density are not significant we consider the flow incompressible.

A flow is described compressible or not from the velocity of the flying object. More specifically, if the Mach number is more than 0.3 we have compressible flow, else the flow is incompressible.

For the compressible problems we can use the Navier – Stokes equations. For an incompressible flow, there are the incompressible Navier – Stokes equations, where:

$$\nabla T = \mu \nabla^2 U \qquad (2.7)$$

whence Eq.2.2 equals to

$$\rho \left(\frac{\partial V}{\partial t} + U \cdot \nabla U \right) = -\nabla p + \mu \nabla^2 U + f \qquad (2.8)$$

and since the density in incompressible flow is constant, with the continuity equation [2] the previous equation (Eq.2.8) turns to the simple form:

$$\nabla \cdot U = 0 \qquad (2.9)$$

As far as the compressible regime, we do not account it unity. For flows with Mach number less than 8, we use the general form of the equations. But for flows with Mach number more than 8, the perfect gas law is not valid, and so the whole flow is different, since the fluid is not ideal anymore.

2.5.4 Viscous or Inviscid flow

Another flow separation is between viscous and inviscid flow. It is the viscosity that separates the two types of flow. When we observe effect from the viscosity we have viscous flow. But when the inertial are much bigger than the viscous one (Re>>1), we consider zero vorticity and Navier Stokes equations are simplified to the Euler equations.

Vorticity (ω) shows the 'rotation' of the fluid. Vorticity is defined as:

$$\omega = \nabla \times U \qquad (2.10)$$

A flow with zero vorticity is called irrotational. For the vorticity field we have:

$$\frac{D\omega}{Dt} = \omega \cdot \nabla U \qquad (2.11)$$

2.5.5 Stokes Flow

When the inertial forces are very small in comparison to the viscous one and so the Reynolds number is low (Re<<1) we can simplify the Navier – Stoke equations to the equation of creeping motion [2]:

$$\nabla p = \mu \nabla U , \qquad (2.12)$$

2.5.6 Potential Flow

In irrotational motion we have that, for an in

$$\omega = \nabla \times U = 0 . \qquad (2.13)$$

For the steady flow Eq.2.11 turns to:

$$\frac{D\omega}{Dt} = \omega \cdot \nabla U = 0 . \qquad (2.14)$$

So we have irrotational flow, since the velocity cannot be zero. We introduce the potential velocity, (ϕ):

$$U = grad\left(\phi\right) \qquad (2.15)$$

So we have from Eq.2.13 that:

$$\nabla^2 \phi = 0 . \qquad (2.16)$$

This shows that potential velocity obeys the Laplace equation.

2.6 Boundary Layers

As the object moves inside a fluid, the molecules of the fluid which are next to the surface of the object stick on the surface. Those molecules collide with the molecules next to them, and this procedure slow down the flow. As the distance of the molecules from the surface increases, this effect (collisions) is less. So a thin layer on the surface of the object is created, where the velocity of the fluid starts from zero (0) on the surface of the object and increases until it is equal to the 99% of the free-stream velocity, where is the end of the layer [1]. This layer, since it is next to the surface of the object, is called boundary layer.
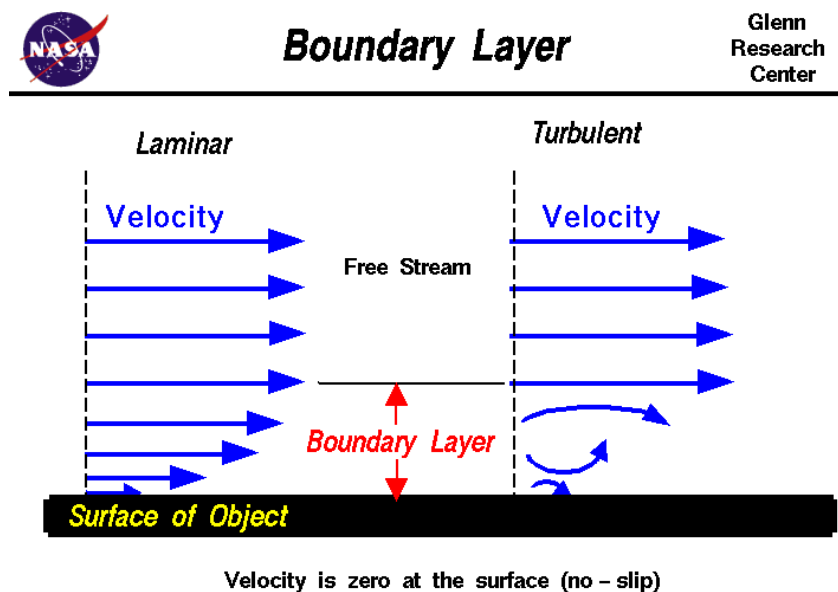
Figure 2.1   Image of a laminar and a turbulent boundary layer [3].

The flow inside a boundary layer can be laminar, turbulent or both. This depends on the velocity, on the angle of attack and on the shape of the object.

The procedure that a laminar boundary layer turns to turbulent boundary layer is called boundary layer transition and the point of the change is denominated as the transition point. As speed increases, the transition point moves forward (at the front edge of the object), and the same happens when the angle of attack increases. But the transition is not a simple procedure. There are 6 stages from laminar to turbulent flow. The transition point is between the 5th and 6th stage. [1, 3].

1. steady laminar flow
2. unsteady Tollmien-Schlichting waves
3. three-dimensional waves and vortex formation (Λ-structures)
4. vortex decay
5. formation of turbulent spots
6. fully turbulent flow
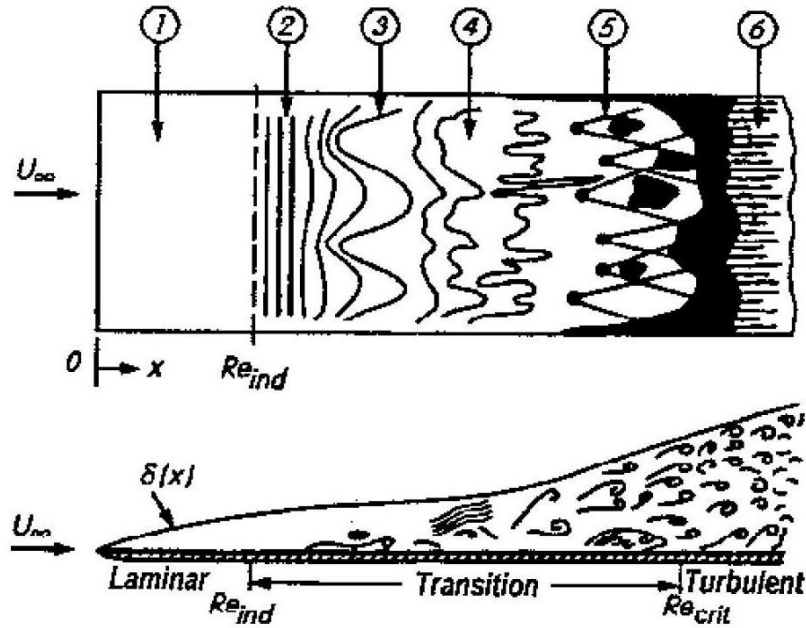
Figure 2.2 Boundary layer transition, from laminar (1) to turbulent (6) flow, on a flat plate, with zero incidence [1]

2.7 Shock Waves

As a flying object accelerates from the subsonic regime to the supersonic one, develops the shock waves, around the object. The field of the shock wave, and how it is created, is depended on the shape of the object, on its velocity (Mach number), and on the angle of attack. The changes at the properties of the fluid are very large, and they are presented at the next equations.

For the angle of the shock wave we have [3]:

$$\cot(\theta_v) = \left(\frac{(\gamma+1)M_0^2}{2(M_0^2 \sin^2(\theta)-1)} - 1 \right) \tan(\theta). \qquad (2.17)$$

For the properties of the fluid, before and after the shockwave, we have for the velocity:

$$M_1^2 \sin^2(\theta - \theta_v) = \frac{(\gamma-1)M_0^2 \sin^2(\theta)+2}{2\gamma M_0^2 \sin^2(\theta)-(\gamma-1)}, \qquad (2.18)$$

for the pressure:

$$\frac{p_1}{p_0} = \frac{2\gamma M_0^2 \sin^2(\theta) - (\gamma - 1)}{\gamma + 1},\tag{2.19}$$

for the temperature:

$$\frac{T_1}{T_0} = \frac{\left[2\gamma M_0^2 \sin^2(\theta) - (\gamma - 1)\right]\left[(\gamma - 1)M_0^2 \sin^2(\theta) + 2\right]}{\left[(\gamma + 1)M_0 \sin(\theta)\right]^2}\tag{2.20}$$

and for the density:

$$\frac{\rho_1}{\rho_0} = \frac{(\gamma + 1)M_0^2 \sin^2(\theta)}{(\gamma - 1)M_0^2 \sin^2(\theta) + 2}.\tag{2.21}$$

As far as the tracking error, we have from the Snell law, and the Gladstone - Dale equation [4]:

$$\sin(\beta_1) = \sin(\beta_0)\frac{n_0}{n_1} = \sin(\beta_0)\left(\frac{1 + G\rho_0}{1 + G\rho_1}\right),\tag{2.22}$$

where ρ, ρ_0 are the densities, and G is the Gladstone-Dale constant., and β is the elevation angle and β_0 the angle of incidence.
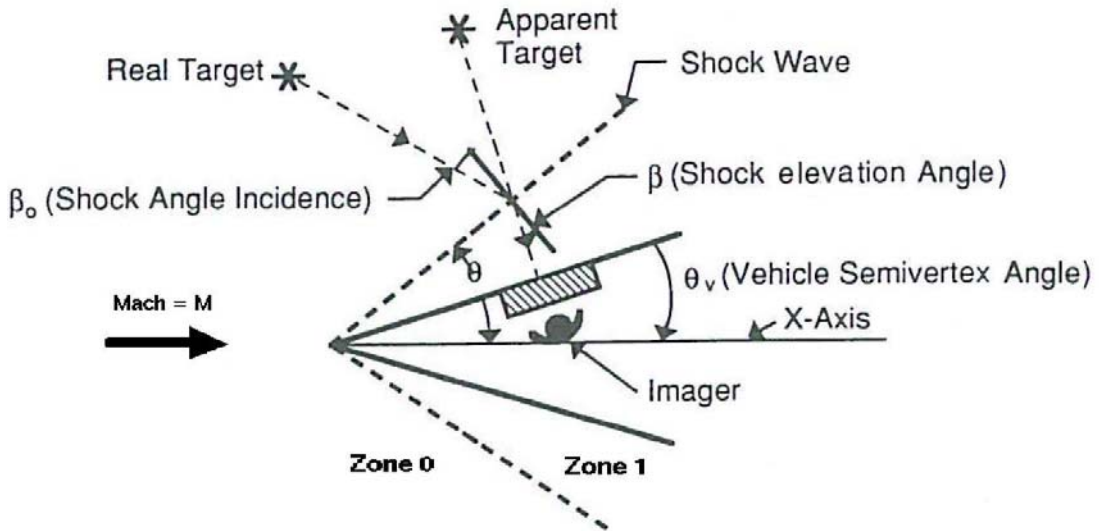
Figure 2.3   We can see a shock wave. Behind it is the free-stream area (Zone 0) and after it, up to the object, is the shock wave area (Zone 1). We can also observe the boresight effects, which are caused by the shock wave. [4]

2.8 Streamline

Streamline is the path that follows a massless objects moving inside the flow. The direction of the velocity is tangent to the curve of the streamline. We can use the Bernoulli equation to relate the velocity and the pressure, along the streamline.

Along the streamline we have:

$$\frac{dx}{u} = \frac{dy}{v} = \frac{dz}{w} \, , \tag{2.23}$$

or

$$u \cdot dy - v \cdot dx = v \cdot dz - w \cdot dy = w \cdot dx - u \cdot dz = 0 \, . \tag{2.24}$$

where u, v, w are the coefficients of the velocity (U).

Figure 2.4 Streamlines over a sphere

2.9 Useful Relationships

Here will be presented some equations of thermodynamics and fluid dynamics that will be used in the following research.

2.9.1 Ideal Gas Law

This law defines the ideal fluids. It is the combination of the 'Boyle' and 'Charles and Gay-Lussac' laws for fluids [3]:

$$p \cdot V = n \cdot R \cdot T \qquad (2.25)$$

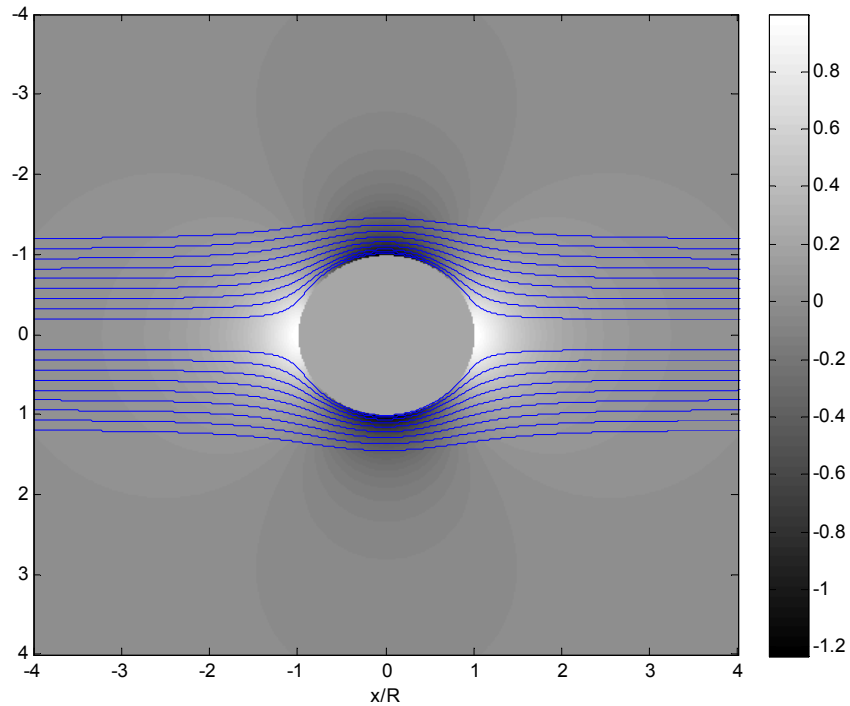where p is the pressure (pa), V is the volume the gas occupies (m^3), n is the moles of gas (mol), R_g is the gas constant $\left(R_g = 8.31432 \ J/(mol \cdot K) \right)$, and T the temperature (K),

or including the density:

$$p = \rho \cdot \overline{R} \cdot T , \qquad (2.26)$$

where $\overline{R}$ is the specific gas constant, which is equal to $\overline{R} = R_g / Moll$, where $Moll$ is the molecular mass.

For dry air, which will be the medium that we use, the molecule mass is 28.964 kg/mol so the specific gas constant is $287.05 \ J/(kg \cdot K)$ [5].

The gas constant, R_g, is equal to the difference between the heat capacity (c) at constant pressure and constant volume of the fluid:

$$R_g = c_p - c_v . \qquad (2.27)$$

The ratio of the heat capacity at constant pressure and constant volume is called adiabatic index:

$$\gamma = \frac{c_p}{c_v} . \qquad (2.28)$$

The adiabatic index is dimensionless and for the air we assume it is equal with 1.4.

2.9.2 Adiabatic Law

Adiabatic process is a thermodynamic process where there is no transferred heat from or to the fluid, in which the process is done, to or from the moving object.

The relationship that describes the adiabatic law is:

$$p \cdot V^{\gamma} = const., \tag{2.29}$$

where V is the volume, and γ is the adiabatic index.

Since the mass is also constant, we have:

$$\frac{p}{\rho^{\gamma}} = const.. \tag{2.30}$$

2.9.3 Bernoulli's Principle and the Bernoulli equation

The Bernoulli's principle says that, in an ideal fluid (ideal gas law is valid), when the velocity increases, the pressure decrease, if there is no heat (energy) transfer. It has a lot of applications, and the most famous is the flight of the airplanes. This principle comes from the Bernoulli equation:

$$p + \frac{1}{2}\rho V^2 = P_t = const. , \tag{2.31}$$

where p is the pressure, ρ is the density, V is the velocity,

Or

$$static\ pressure\ +\ dynamic\ pressure\ =\ total\ pressure \tag{2.32}$$

where p is the static pressure, $(1/2)\rho V^2$ is the dynamic pressure and P_t is the total pressure, which is constant for ideal fluids.

2.9.4 Pressure Coefficient

The fluid performance around the flying object will be studied from the variation of the fluid properties, but more easily from the pressure. Pressure will be expressed

through the dimensionless pressure coefficient, C_p, which shows the aberrance of the pressure around the object from the free stream pressure $(p - p_\infty)$. It is defined as:

$$C_p = \frac{p - p_\infty}{\frac{1}{2}\rho_\infty \cdot U^2}.$$ (2.33)

From [6] we have:

$$\frac{p - p_\infty}{\rho_\infty} = -\delta\left(\frac{1}{2}U^2 + \frac{\partial\Phi}{\partial t}\right) = -\left[\frac{1}{2}\left(U^2 - U_\infty^2\right) + \frac{\partial\Phi}{\partial t}\right] = \frac{1}{2}\left(U_\infty^2 - U^2\right) + \frac{\partial\Phi}{\partial t}.$$ (2.34)

For steady flows, from Eq.2.6 exists: $\partial\Phi/\partial t = 0$, so the pressure coefficient equals to:

$$C_p = \frac{p - p_\infty \big/ \rho_\infty}{\frac{1}{2}\cdot U_\infty^2} = \frac{\frac{1}{2}\left(U_\infty^2 - U^2\right)}{\frac{1}{2}\cdot U_\infty^2} = 1 - \left(\frac{U}{U_\infty}\right)^2,$$ (2.35)

where U is the velocity in one point and U_∞ is the free-stream velocity.

2.9.5 Other Equations of Fluid Dynamics

The definition of the velocity of the air α is:

$$\alpha^2 = \frac{dp}{d\rho},$$ (2.36)

From the adiabatic law we have:

$$\alpha^2 = \frac{\gamma \cdot p}{\rho},$$ (2.37)

or from the ideal gas law, speed of the air depends only on the temperature:

$$\alpha = \sqrt{\gamma \cdot \overline{R} \cdot T},$$ (2.38)

where ϑ is the temperature in K, γ is dimensionless, $\overline{R}$ is in $J/(kg \times K)$ and so (α) is in m/s.

Mach number is the ratio of the velocity of one object, U, to the speed of sound of the air at that point:

$$M = \frac{U}{\alpha}.$$
(2.39)

So from Eq.2.37 and Eq.3.39 , Mach number equals to:

$$M^2 = \frac{\rho U^2}{\gamma p},$$
(2.40)

whence the pressure coefficient equals to:

$$C_p = \frac{p - p_\infty}{\frac{\rho_\infty}{2} \cdot U_\infty^2} = \frac{p - p_\infty}{\frac{\gamma}{2} \cdot M_\infty^2 \cdot p_\infty}.$$
(2.41)

From the Bernoulli equation we have [7]:

$$\frac{\gamma}{\gamma - 1} \frac{p}{\rho} + \frac{1}{2} U^2 = const = \frac{\gamma}{\gamma - 1} \frac{P}{\rho_0}.$$
(2.42)

From the previous equation and the adiabatic law, we have:

$$\frac{P_t}{p} = \left(1 + \frac{\gamma - 1}{2} M^2\right)^{\frac{\gamma}{\gamma - 1}}.$$
(2.43)

For two points A, B with the previous equation we have the pressure ratio for those points:

$$\frac{p_A}{p_B} = \frac{P_t / p_B}{P_t / p_A} = \left(\frac{1 + \frac{\gamma - 1}{2} M_B^2}{1 + \frac{\gamma - 1}{2} M_A^2}\right)^{\frac{\gamma}{\gamma - 1}}.$$
(2.44)

If we set $M_A = M$ and $M_B = M_\infty$ and we loose the equation for M, we have

$$M = \sqrt{\frac{2}{\gamma - 1} \cdot \left[\frac{1 + \frac{\gamma - 1}{2} \cdot M_\infty^2}{\left(1 + \frac{\gamma}{2} \cdot M_\infty^2 \cdot C_p\right)^{\frac{\gamma - 1}{\gamma}}} - 1\right]},$$
(2.45)

since from the pressure coefficient:

$$\frac{p}{p_\infty} = 1 + \frac{\gamma}{2} M_\infty^2 C_p.$$
(2.46)

From the adiabatic law and the pressure ratio (Eq.2.44) we have the density ratio:

$$\frac{\rho_A}{\rho_B} = \left(\frac{p_A}{p_B}\right)^{1/\gamma} = \left(\frac{1 + \frac{\gamma-1}{2} M_B^2}{1 + \frac{\gamma-1}{2} M_A^2}\right)^{\frac{1}{\gamma-1}}$$
(2.47)

3

Air and Air conditions

3.1 Introduction

In this chapter we examine the characteristics of the air, where the simulation is done. The fluid property, which determines the fluctuations of the beam wavefront, is the refractive index. Let $n(x,y,z)$ the refractive index in the 3-dimensional space. The optical path length, noted *OPL*, is related to the refractive index by

$$OPL(x,y,z) = \int_0^y n(x,y,z)dy \, . \tag{3.1}$$

So we have to calculate the variation of the refractive index around the flying object. In order to achieve that, we have to know the composition of the air, and the causes that can change the refractive index.

3.2 Refractive Index

The refractive index *n* of a medium is defined as the ratio of the velocity of one electromagnetic wave in vacuum c_0 to the velocity of the wave in this medium *c*:

$$n = \frac{c_0}{c} \, . \tag{3.2}$$

It is related with the density and so with the other properties of the medium, through the Gladstone – Dale relationship [8]:

$$G = \frac{n-1}{\rho} \, , \tag{3.3}$$

Or
$$n = 1 + \rho \cdot G \, , \tag{3.4}$$

where *G* is the Gladstone – Dale constant and ρ is the density of the medium.

If we adapt the mean values to the Eq. 3.4 we have $\mu_n = 1 + \mu_\rho \cdot G$, where μ are the mean values, and since $n' = n - \mu_n$ and $\rho' = \rho - \mu_\rho$ are the fluctuating values for the refractive index and the density, we have the relationship [4]:

$$n' = G \cdot \rho'. \tag{3.5}$$

In Figure 3.1 is presented the wavelength dependence of the Gladstone – Dale constant, according to the equation (λ in microns) [9]:

$$G(\lambda) = \left(2.192539 + \frac{0.01785076}{\lambda^2} \right) \times 10^{-4} \tag{3.6}$$
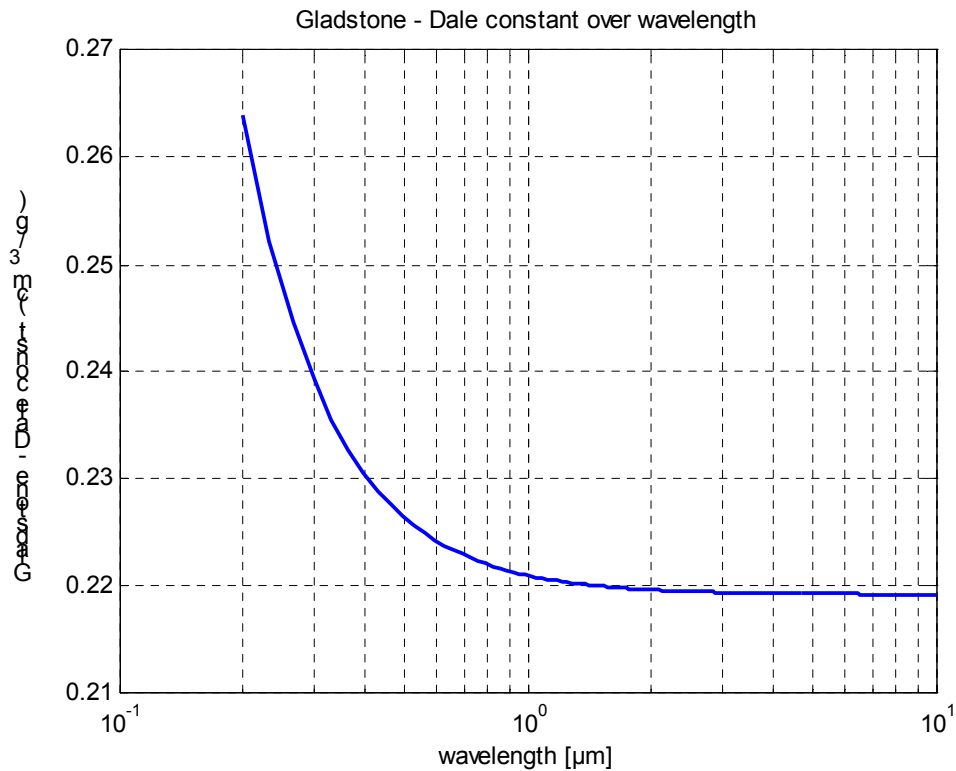
Figure 3.1   the Gladstone-Dale constant over the wavelength

It is obvious from Eq.3.3 that for a specific wavelength we have a constant ratio between the density and the aberrance of refractive index from one, for two different points of the medium:

$$\frac{\rho_A}{\rho_B} = \frac{n_A - 1}{n_B - 1}. \tag{3.7}$$

That shows us that if we know the density ratio between two points (Eq.2.47), and the refractive index in one of them (it can be at the free-stream area), we can calculate the refractive index at the other point. So we have to define the free-stream properties. Of course the fluid that we consider is dry air.

3.3 Models for Conditions of the Air at the Free-stream Area

Dry Air is considered an ideal fluid, so we can calculate of the density through the perfect gas law:

$$p = \rho \cdot \overline{R} \cdot T \quad , \tag{3.8}$$

In our research we will use three standard conditions for the value of temperature and pressure of the air.

The velocity will be expressed trough the Mach number. From the previous chapter (Eq.2.38) we have seen that the value of the speed of the air is related only to the temperature. So we can also calculate the value of the Mach number for each model that we will use.

3.3.1 Standard Temperature and Pressure

The first air properties model is the Standard Temperature and Pressure (STP). The values for the two variables are constant and equal with 1 bar (10^5 Pa) for the pressure and 273.15 K (0 °C) for the temperature. In this case we can calculate the density from Eq.3.10 which equals with $\rho_{STP} = 1.2754 \ kg/m^3$ [3]. From Eq.2.38 we have for the speed of the air equals to 331.31.

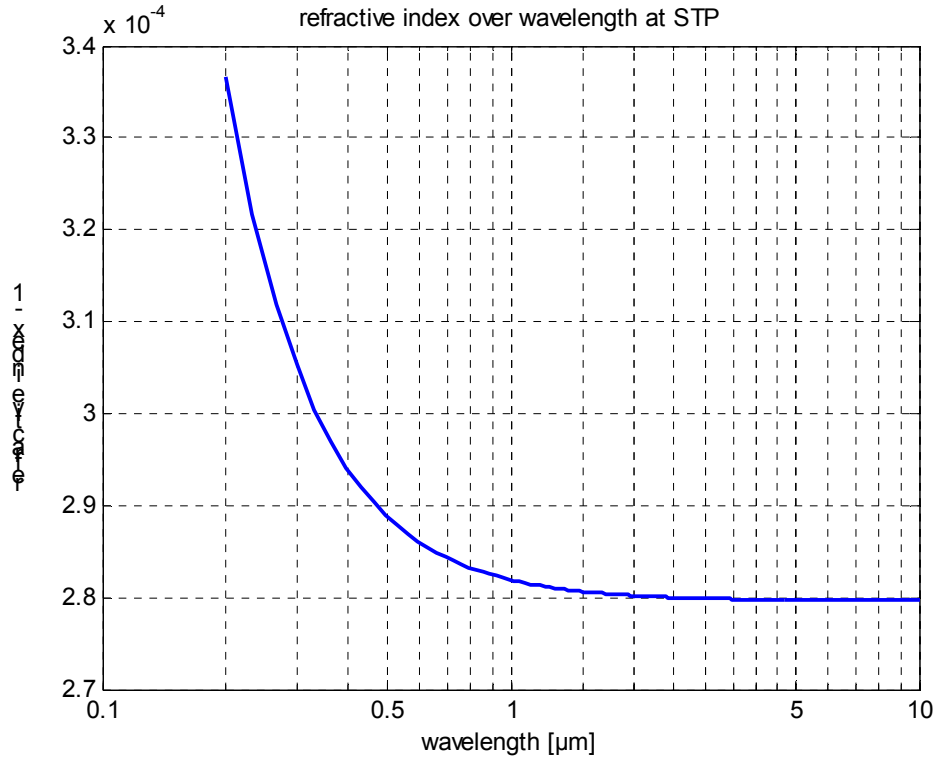According to the Figure 3.1 we can find the refractive index at STP for wavelengths from 0.2 until 10 μm.

Figure 3.2 the refractive index over the wavelength for standard temperature and pressure.

3.3.2 ISA Model

The second model we will use for the free-stream properties is the model of International Standard Atmosphere (ISA), published in 1975, presented at Table 3.1 and Figures 3.3 – 3.5. This is a model of how the temperature, the pressure and the density of Earth's atmosphere change over the altitude. Since we know the properties of the air along the altitude, we can calculate, for a specific height and wavelength, the refractive index. This model is similar to other standard atmospheric models, such as the "International Civil Aviation Organization" (ICAO) model, or the "US Standard Atmosphere", 1976 [10].

Layer	Level Name	Geopotential Height (km)	Temperature (K)	Pressure (pa)
1	Troposphere	0	288.15	101325
2	Tropopause	11	216.65	22632
3	Stratosphere	20	216.65	5474.9
4	Stratosphere	32	228.65	868.02
5	Stratopause	47	270.65	110.91
6	Mesosphere	51	270.65	66.939
7	Mesosphere	71	214.65	3.9564
8	Mesopause	84.852	186.95	0.3734

Table 3.1   the values of the ISA-model.

3.3.3 Barometric Formula

We have seen at the previous paragraph how the properties of the air change along the height. But with this method we have values only for 8 different heights. There is another method, named Barometric Formula, where using the previous model, the properties change also inside the areas of the given heights.

b	Geopotential Height (km) $-h_b-$	Temperature (K) $-T-$	Pressure (pa) $-p-$	Temperature Lapse Rate (K/m) $-L_b-$	Density (kg/m^3) $-\rho-$
0	0	288.15	101325	-0.0065	1.225
1	11	216.65	22632	0	0.36391
2	20	216.65	5474.9	0.001	0.08803
3	32	228.65	868.02	0.0028	0.01322
4	47	270.65	110.91	0	0.00143
5	51	270.65	66.939	-0.0028	0.00086
6	71	214.65	3.9564	-0.002	0.000064

Table 3.2   the values for the Barometric Formula

The equations of the formula are the following:

For the pressure, when $L_b \neq 0$:

$$p = p_b \left[\frac{T_b}{T_b + L_b \cdot (h - h_b)} \right]^{\frac{g_0 \cdot M}{R \cdot L_b}} \tag{3.9}$$

and when $L_b = 0$:

$$p = p_b \cdot \exp\left[\frac{g_0 \cdot M \cdot (h - h_b)}{R \cdot T_b}\right]. \tag{3.10}$$

For the density, the equations are similar. When $L_b \neq 0$:

$$\rho = \rho_b \left[\frac{T_b}{T_b + L_b \cdot (h - h_b)}\right]^{\frac{g_0 \cdot M}{R \cdot L_b}}, \tag{3.11}$$

and when $L_b = 0$:

$$\rho = \rho_b \cdot \exp\left[\frac{g_0 \cdot M \cdot (h - h_b)}{R \cdot T_b}\right]. \tag{3.12}$$

We can calculate also the temperature, from the perfect gas law. Then from Eq.2.38 we are able to find the value of the speed of the air (1 Mach) along the height.

The next Figures (3.3 - 3.5) depict these two models. We observe that the barometric formula is more specific than the atmospheric model, and we will use this formula for our calculations. We are interested in heights until 30 km, since after that height flying is impossible.
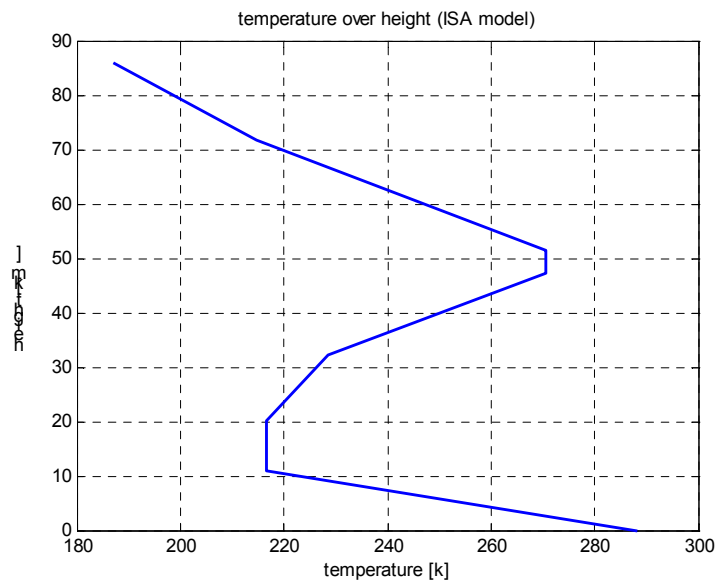
Figure 3.3 presents the temperature over the height according to the atmosphere model of ISA (1976).
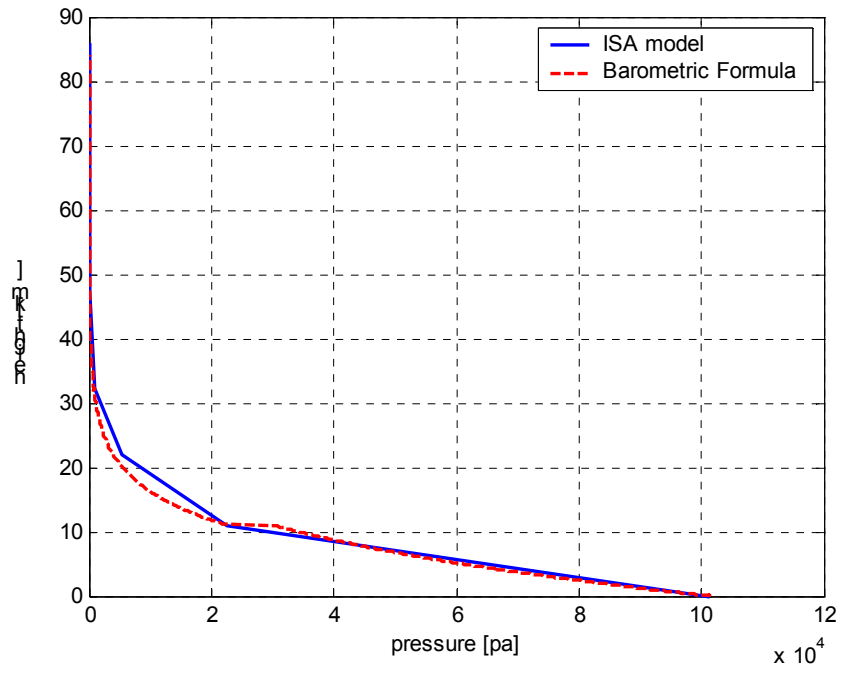
Figure 3.4 presents the pressure over the height
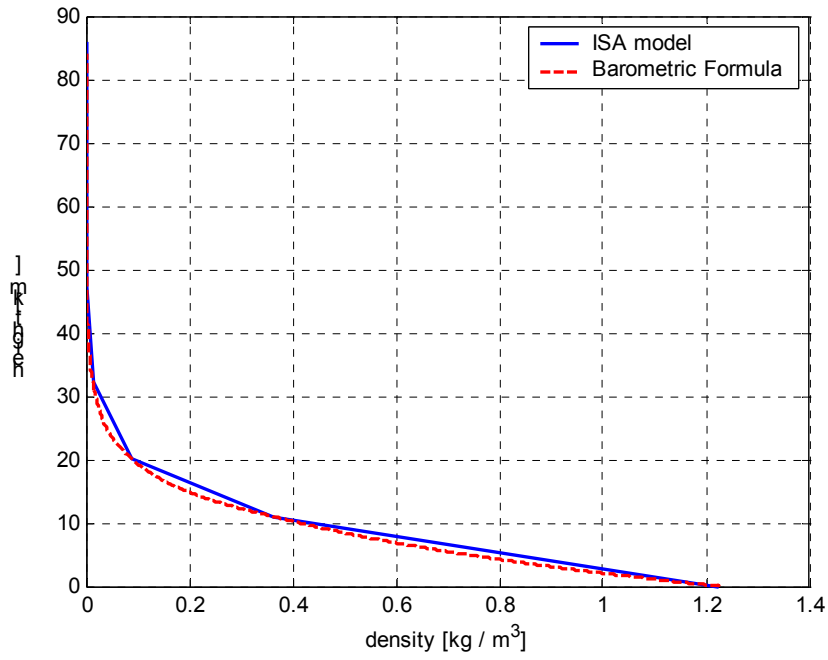
Figure 3.5 presents the density over the height

3.4 Refractive Index over Height

We have seen that the refractive index is related to the height through the density. In this paragraph we will find the relation of the refractive index and the height, with three different methods. In the first two we will use the Barometric Formula, and in the third one there is a direct dependence of the refractive index on the height.

3.4.1 Method A

From Eq.3.4 we observe that, since we know the density for each height, we are able to find the refractive index, along the altitude, for one specific wavelength (from the Gladstone-Dale equation). We can use Figure 3.5 in order to find the density over the altitude.

3.4.2 Method B

Another way to calculate the refractive index is with the following equation [11]:

$$n = 1 + 77.6 \times 10^{-6} \cdot \left(1 + 7.52 \times 10^{-3} \times \lambda^{-2}\right) \cdot \frac{p}{T},$$ (3.13)

where λ the optical wavelength in μm, p is the pressure in millibars (mbar), and T is the temperature in Kelvin.

Here we will use the values the barometric formula. We have to notice, that from the ideal gas law, Eq.3.8, we have that $p/T = \rho \cdot \overline{R}$.

3.4.3 Method C

The last equation between the refractive index and the altitude is [12]:

$$n = 1 + n_d \cdot e^{-y/H},$$ (3.14)

where n is the refractive index, y is the height in meters, H a scale height with value 7400m, and n_d the differential refractive index, which depends on the wavelength (in meters):

$$n_d = 2.879 \cdot 10^{-4} + 2.165 \cdot 10^{-18} \cdot \lambda^{-2} . \qquad (3.15)$$

All three methods are presented in Figure 3.6, in order to compare them. The calculations have been for the wavelength: $\lambda = 1550nm$.
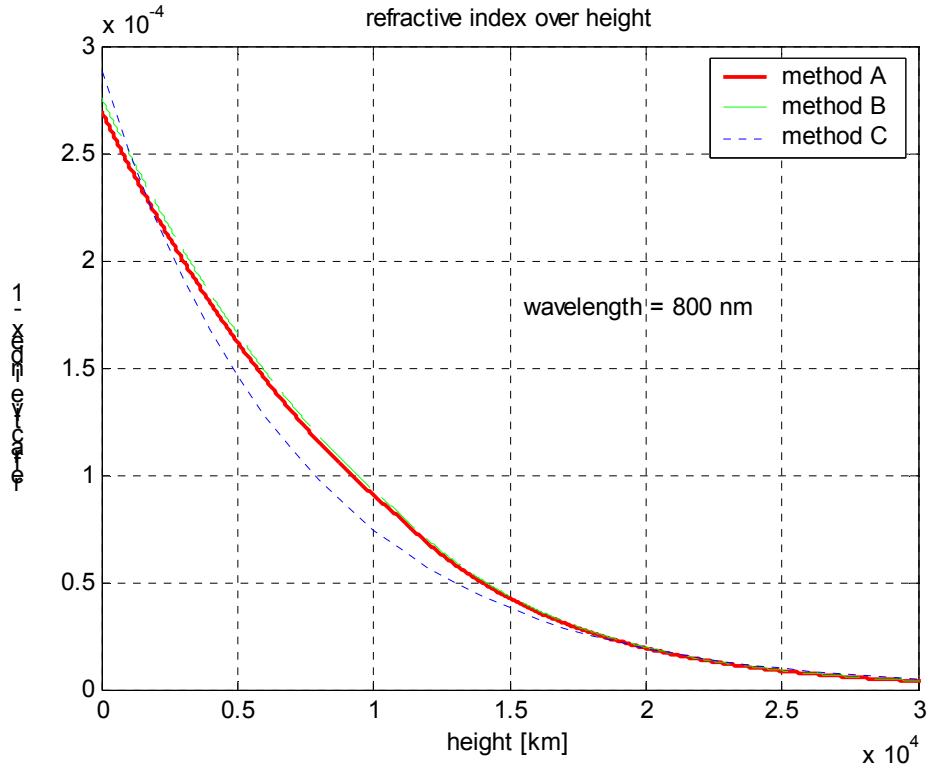
Figure 3.6   shows the refractive index along the height, for every height, that is able to fly (< 30 km). The three lines are for $\lambda = 1550nm$, so we can compare the results of the three methods.

From the three different methods we will use the first one (method A), since it is not a formula, but it comes from the definitions of the variables we use.

4

Flow around a Sphere

4.1 Introduction

In this chapter we will investigate the wavefront of a laser beam. We assume there is a spherical flying object, which we consider as the turret. In the turret will be a concentric circular aperture. The flow is steady, laminar, and incompressible. The Reynolds number is very small we have potential flow. For this case we will find the velocity field around a sphere. Then we can calculate the pressure coefficient, and for certain free-stream conditions the pressure. From the pressure, we can calculate the density and then at the refractive index through the Gladstone – Dale relationship, creating the OPD. From OPD we calculate the Zernike coefficients, which describe the wavefront and the OPD_{rms}. From OPD we also calculate the phase error, and then the boresight error (Figure 4.1). The mean boresight error is the mean tilt of the wavefront.

In order to calculate the final distortions, we have to mind several properties (pressure, density, refractive index), whose values are depended from many other variables such as the ratio between the diameters of the aperture and the turret, the velocity of the sphere (Mach number), as well as the elevation angle of the beam, and the height that the sphere is (§ 2.3.2). Since the flying object is a sphere, the angle of attack of the turret is always the same. In the following pages there are calculations for

- Different diameter ratio between the turret and the aperture
- Different elevation angle
- Different mach number
- Different altitude

Finally we have to know the wavelength of the beam. For optical communication, the typical values of the wavelength are 800, 1064, 1550 nm. In the results of the simulation we will compare of the results for wavelengths of 800nm and 1550nm. The results of a beam at 1064nm will be in the area of the results of the other two wavelengths (Figures 4.10 & 4.11).

wavelength (nm)	refractive index
800	1.0002831
1064	1.0002816
1550	1.0002805

Table 4.1 The refractive index of air at STP for three standard wavelengths of laser beams

Velocity

$$C_p = 1 - \left(\dfrac{U}{U_\infty}\right)$$

Pressure Coefficient

$$M = \sqrt{\dfrac{2}{\gamma-1} \cdot \left[\dfrac{1+\dfrac{\gamma-1}{2}\cdot M_\infty^{\,2}}{\left(1+\dfrac{\gamma}{2}\cdot M_\infty^{\,2}\cdot C_p\right)^{\frac{\gamma-1}{\gamma}}}-1\right]}$$

Mach Number

$$\dfrac{\rho}{\rho_\infty} = \left(\dfrac{1+\dfrac{\gamma-1}{2}\cdot M_\infty^{\,2}}{1+\dfrac{\gamma-1}{2}\cdot M^2}\right)^{\frac{1}{\gamma-1}}$$

Density

$$n = 1 + \rho \cdot G$$

Refractive Index

$$OPL(x,y) = \int_R^L n(x,y,z)\,dz$$

OPL

$$OPD = OPL - OPL_{min}$$

OPD

$$e(x,y) = \dfrac{2\pi}{\lambda}\cdot OPL(x,y)$$

$$OPD = \dfrac{1}{S}\sqrt{\int\left(OPL - \overline{OPL}\right)dx\cdot dy}$$

Phase Error

Zernike Polynomial

$$OPD_{RMS}$$

$$a(x,y) = -\dfrac{\lambda}{2\pi}\cdot\dfrac{\partial}{\partial(x,y)}e(x,y)$$

Boresight Error

Mean Tilt
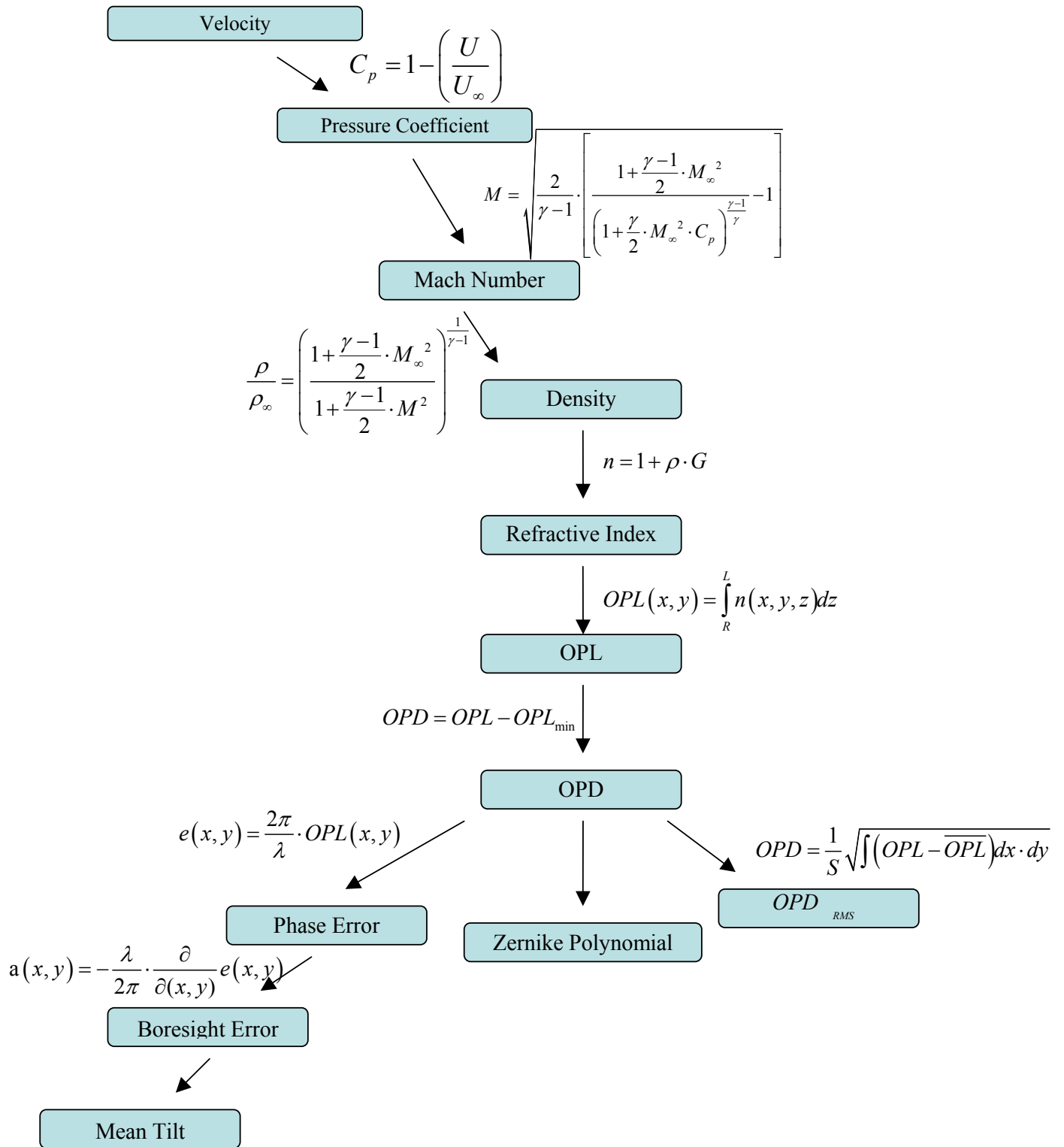
Figure 4.1 Diagram of the method for the calculation of the wavefront fluctuations

Reynolds number regime	Flow regime	Flow form	Flow characteristic	Strouhal number Sr	Drag coefficient c_D	Separation angle Θ_S
$Re \to 0$	Creeping flow		Steady, no wake	–	see Fig. 1.12	–
$3-4 < Re < 30-40$	Vortex pairs in wake		Steady, symmetric separation	–	$1.59 < c_D < 4.52$ (Re = 30) (Re = 40)	$130° < \Theta_S < 180°$ (Re = 35) (Re = 5)
$30/40 < Re < 80/90$	Onset of Karman vortex street		Laminar, unstable wake	–	$1.17 < c_D < 1.59$ (Re = 100) (Re = 30)	$115° < \Theta_S < 130°$ (Re = 90) (Re = 35)
$80/90 < Re < 150/300$	Pure Karman vortex street		Karman vortex street	$0.14 < Sr < 0.21$		
$150/300 < Re < 10^6/1.3 \cdot 10^6$	Subcritical regime		Laminar, with vortex street instabilities	$Sr \approx 0.21$	$c_D \approx 1.2$	$\Theta_S \approx 80°$
$10^5/1.3 \cdot 10^6 < Re < 3.5 \cdot 10^6$	Critical regime		Laminar separation Turbulent reattachment Turbulent separation Turbulent wake	No preferred frequency	$0.2 < c_D < 1.2$	$80° < \Theta_S < 140°$
$3.5 \cdot 10^6 < Re$	Supercritical regime (transcritical)		Turbulent separation	$0.25 < Sr < 0.30$	$c_D \approx 0.6$	$\Theta_S \approx 115°$

Figure 4.2 Types of flow around a cylinder. The flow around a cylinder is very similar to the flow around a sphere [1].

4.2 Flow around a sphere

In this thesis we will investigate the flow around a sphere. We know that this flow is very similar to the flow around a cylinder. In Figure 4.2 we can see the different stages, from laminar to the turbulent flow around a cylinder. We will describe the first case of the flow.

The flow is described as steady, laminar, incompressible. Since the flow is incompressible the velocity must be below 0.3 Mach. But the Reynolds number is very small (Re → 0). We set the critical Reynolds number that we have this flow to 0.2 []. From Eq.2.5 we know that the Reynolds number is proportional to the velocity of the object as well as to the characteristic length. For a sphere the characteristic length is its radius. In Figures 4.3, 4.4 we can see which should be the diameter of the sphere over different velocities, in order to have this kind of flow. We see that the diameter is very small.
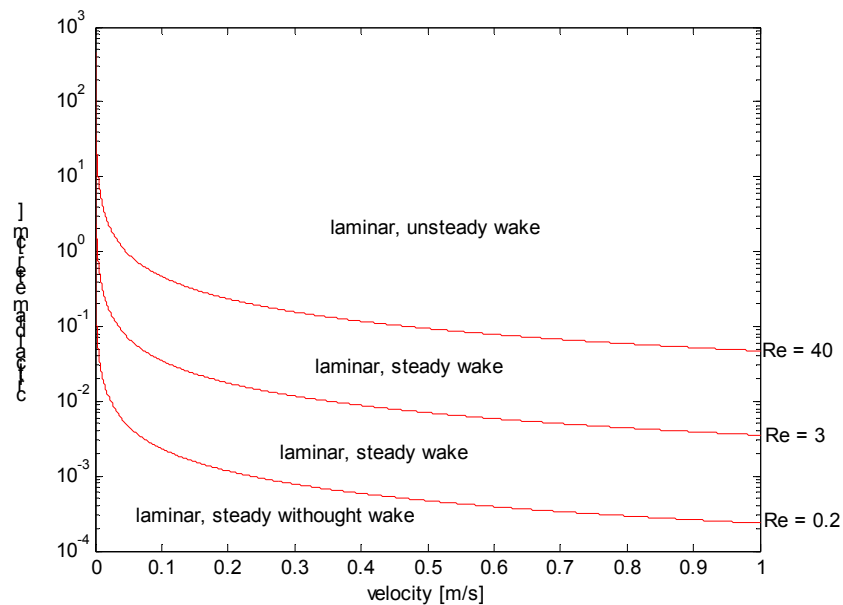
Figure 4.3 Velocity (m/s) over diameter of a sphere for several Reynolds numbers and kinds of flow
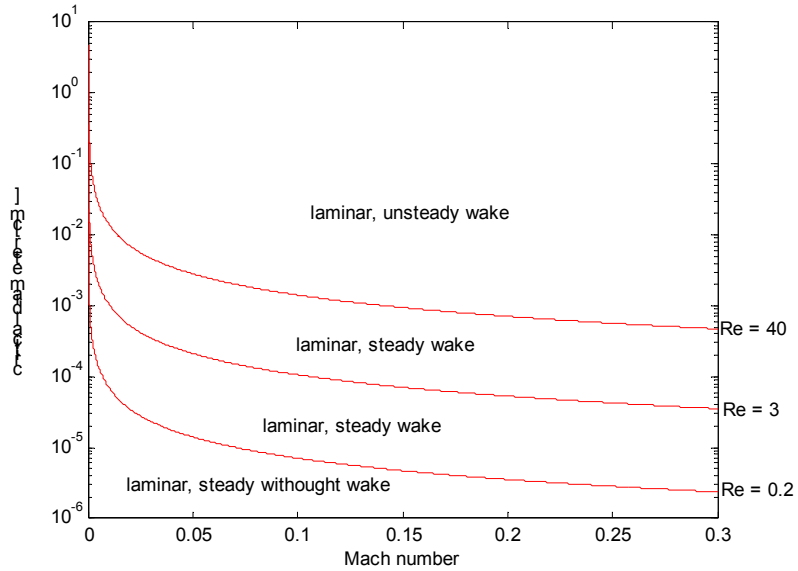
Figure 4.4 Velocity (Mach number) over diameter of a sphere for several Reynolds numbers and kinds of flow

4.3 Steady, Laminar, Incompressible Flow around a Sphere

From §2.2 we have that the potential velocity obeys the Laplace equation:

$$\nabla^2 \phi = 0 \qquad (4.1)$$

Solving this equation for a sphere (3 coordinates) we get:

$$\phi = U_\infty \left(1 + \frac{R^3}{r^3} \right) x , \qquad (4.2)$$

where R is the radius of the sphere, and r the distance of one point from the centre of the sphere, x is the x-coordinate.

Since for the potential velocity we have, Eq.2.15: $U = grad(\phi)$, we can find the three coordinates of the velocity *(u, v, w)* at the Cartesian coordinate system *(x ,y ,z)*.

$$u = \frac{\partial \phi}{\partial x} = U_\infty \cdot \left[1 + \frac{1}{2} \cdot \frac{\left(\dfrac{r}{R}\right)^2 - 3 \cdot \left(\dfrac{x}{R}\right)^2}{\left(\dfrac{r}{R}\right)^5} \right] , \qquad (4.3)$$

$$v = \frac{\partial \phi}{\partial y} = -\frac{3}{2} \cdot U_\infty \cdot \frac{\left(\frac{x}{R}\right) \cdot \left(\frac{y}{R}\right)}{\left(\frac{r}{R}\right)^5} , \tag{4.4}$$

$$w = \frac{\partial \phi}{\partial z} = -\frac{3}{2} \cdot U_\infty \cdot \frac{\left(\frac{x}{R}\right) \cdot \left(\frac{z}{R}\right)}{\left(\frac{r}{R}\right)^5} , \tag{4.5}$$

So we calculate the pressure coefficient (Eq.2.35):

$$C_p = 1 - \left(\frac{U}{U_\infty}\right)^2 = 1 - \left[\left(\frac{u}{U_\infty}\right)^2 + \left(\frac{v}{U_\infty}\right)^2 + \left(\frac{w}{U_\infty}\right)^2\right] \tag{4.6}$$

With the following equations we can have the pressure coefficient around the sphere, at three dimensions. Because of the symmetry over y- and z- axis, we set z = 0 => w = 0, and we have a two dimensional Figure which is a section crossing from the centre of the sphere. Because of the symmetry every centre-crossing section, rotating on the x-axis has the same conFiguration (Figure 4.5).

We have to notice that there is no influence on the pressure coefficient, from the velocity of the object (Mach number) as well as the radius of the turret. It depends only at the ratio of the distance of one point from the centre of the sphere to the radius of the sphere (r/R). At Figure 4.6 we can see the pressure coefficient on the surface of the sphere.

Knowing the pressure coefficient in one point, we can find there the Mach number, as well as the density ratio.

The Mach number and the density ratio in that point equals with (Eq.2.45, Eq.2.47):

$$M = \sqrt{\frac{2}{\gamma-1} \cdot \left[\frac{1 + \frac{\gamma-1}{2} \cdot M_\infty^2}{\left(1 + \frac{\gamma}{2} \cdot M_\infty^2 \cdot C_p\right)^{\frac{\gamma-1}{\gamma}}} - 1\right]} , \tag{4.7}$$

$$\frac{\rho}{\rho_\infty} = \left(\frac{1 + \frac{\gamma-1}{2} \cdot M_\infty^2}{1 + \frac{\gamma-1}{2} \cdot M^2}\right)^{\frac{1}{\gamma-1}} . \tag{4.8}$$
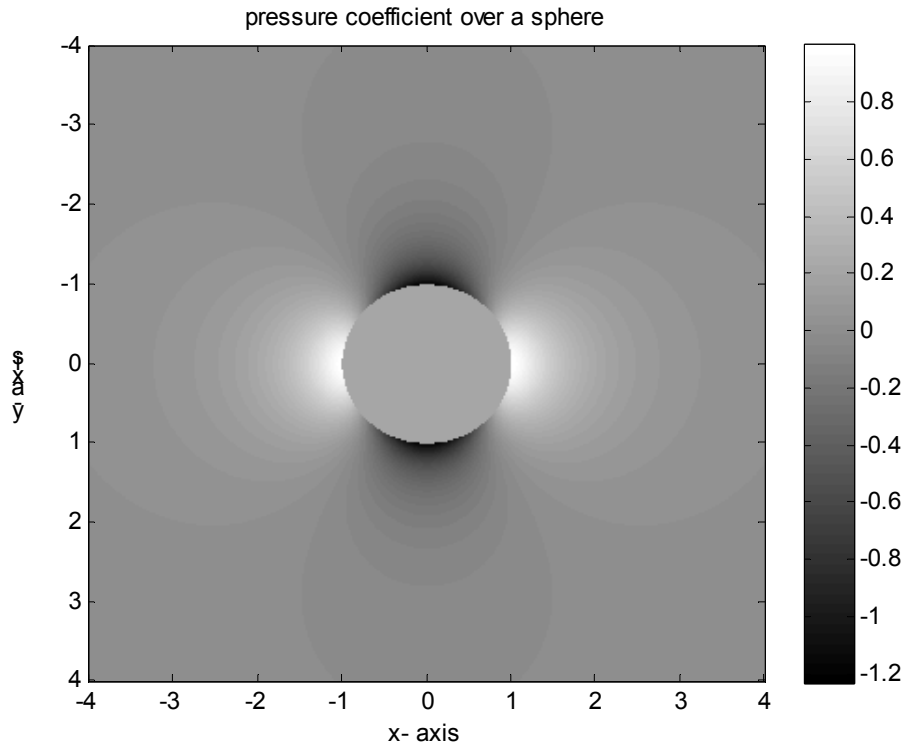
Figure 4.5 The pressure coefficient around a flying sphere in a 2-D diagram. There is symmetry over y- and z- axis (y ≡ z), so here z = 0.
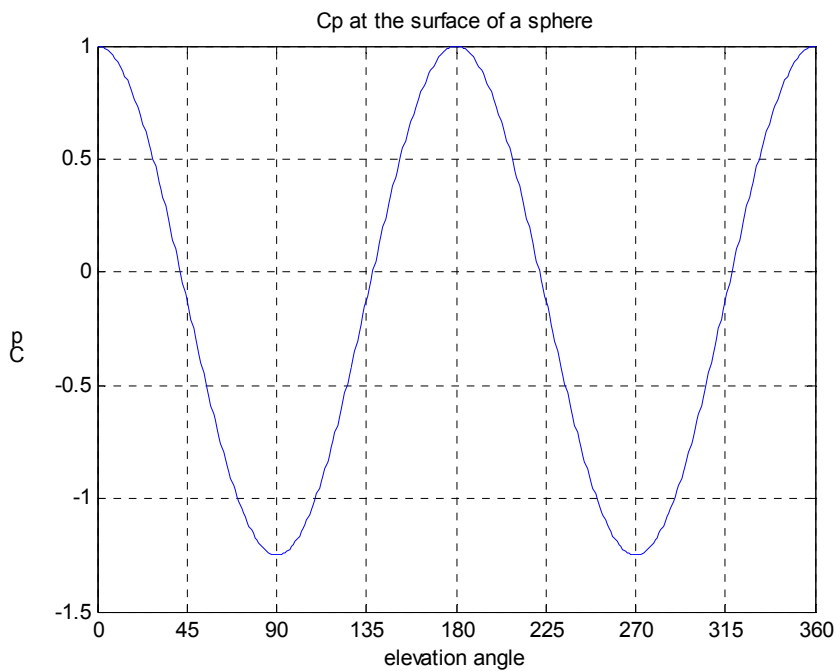
Figure 4.6 The pressure coefficient on the surface of a sphere. It is independent from the radius of the sphere, as well as the Mach number: $C_p = 1 - (9/4)\sin^2(\theta)$.
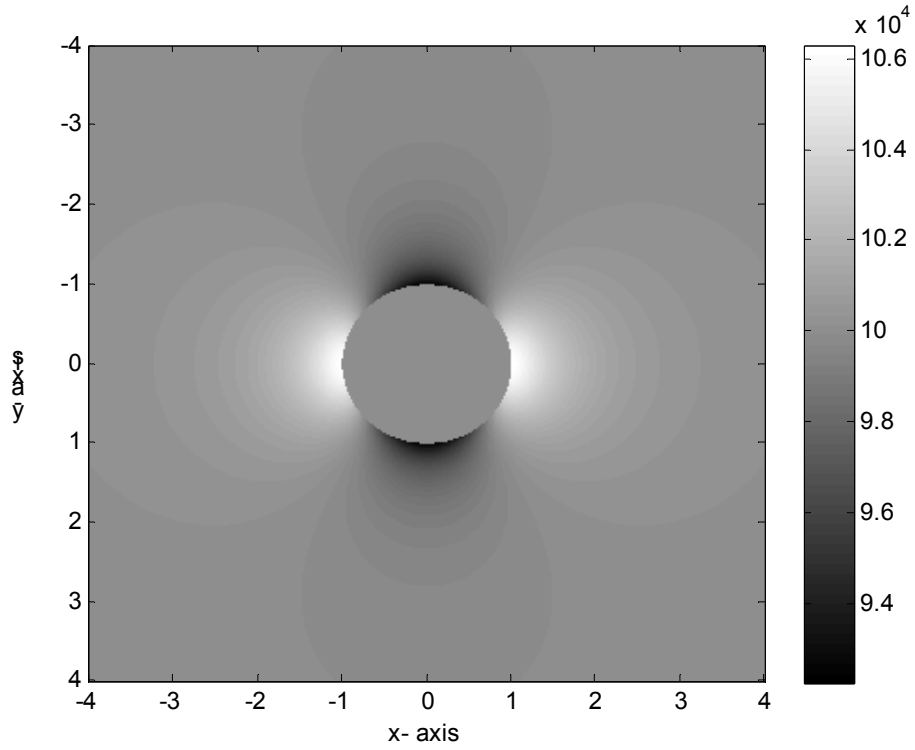
Figure 4.7 Pressure around a flying sphere (R = 1) in Pascal, for free stream Mach number = 0.3 and free stream pressure = 10^5 pa (STP).
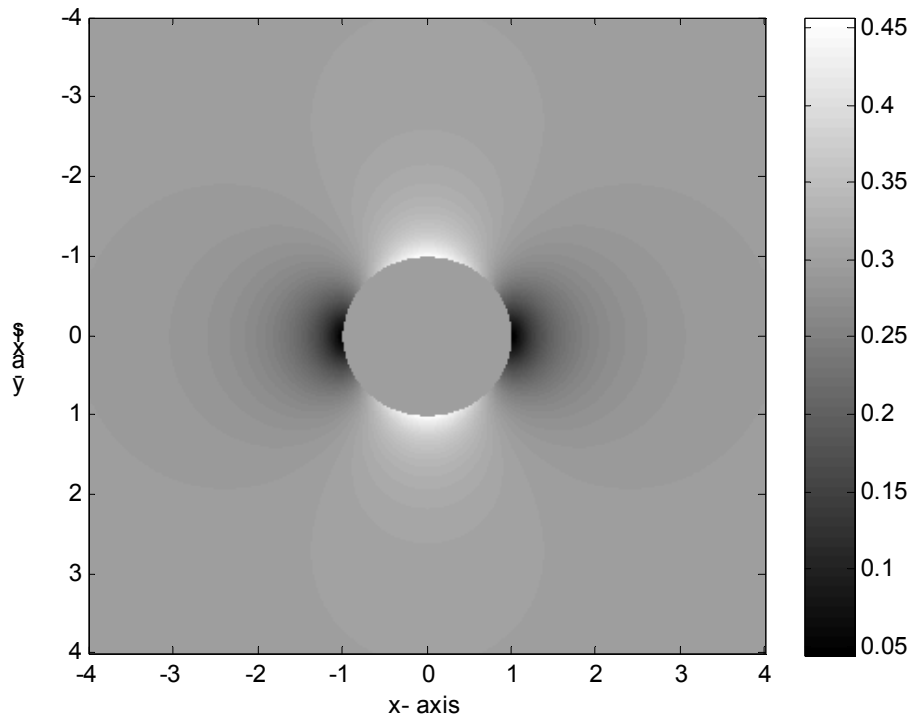
Figure 4.8 Mach number around a flying sphere, with free stream Mach number = 0.3.
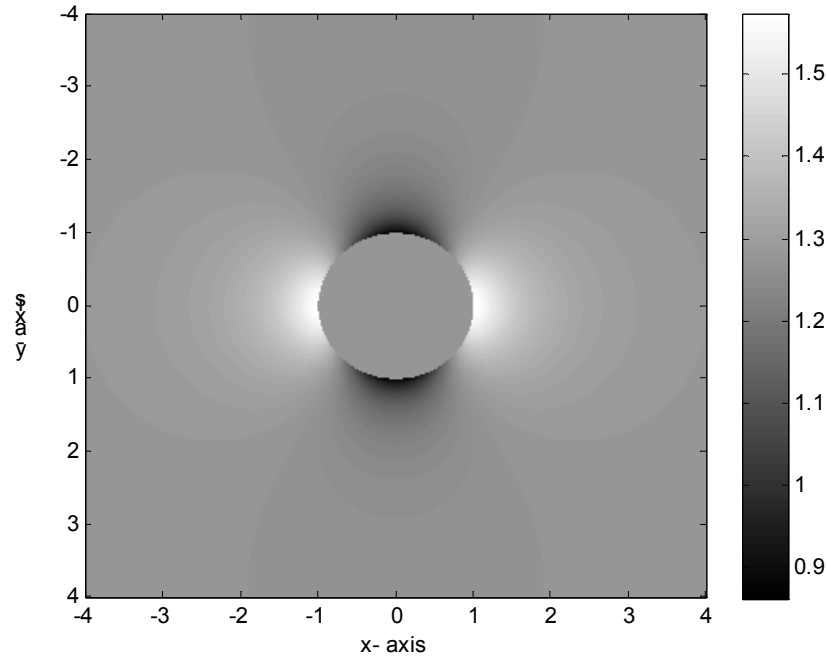
Figure 4.9 Density around a flying sphere. Free stream density is $\rho_{STP} = 1.2754 \; kg/m^3$ (§2.3.1).

4.4 Optical Length of Centre Crossing Paths

Knowing the density ratio (4.8) and the free-stream air properties we can find the refractive index (3.7) at any point, and after the OPL and the OPD (3.1).

We have the same turret as before, with radius R. The calculated path starts at a radial distance R, and ends at a radial distance $L = 10 \times R$, from the centre of the turret. It ends there because we observe that after this radius, there is almost no difference at the value of OPL. The wavelength of the beam is 1550nm. The fluid is air at STP and the free-stream Mach number is 0.3. At Figure 4.10 we have the diagram of the factor of OPL for angles from 0° until 180°, since there is symmetry for the angles from 180° to 360°. In order to observe the fluctuation of OPL, we normalize it, at Figure 4.11, and have the factor of OPD (Optical Path Difference), which is defined as

$$OPD = OPL - OPL_{min} . \tag{4.9}$$

The factor of OPL and OPD is the ratio of the optical path and the radius of the sphere and equals to:

$$factor = \frac{OP}{R} . \tag{4.10}$$

Both pictures depict that there is symmetry, with symmetry-axes at 90°, where is also the minimum of the OPL. At the angles 0°, 180° is the peak.
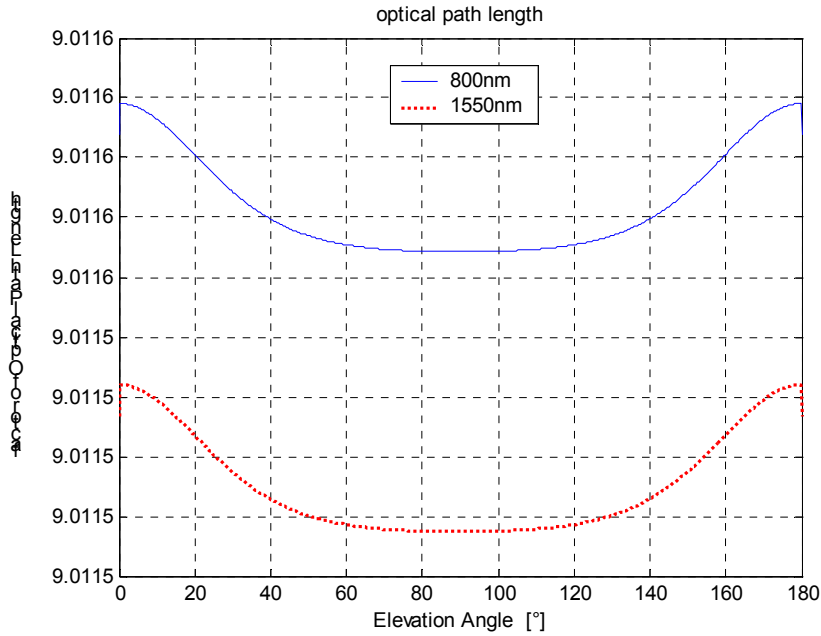
Figure 4.10 factor of OPL for a sphere, with radius R, Mach number is M = 0.3 and air is at STP, for beams of 800nm and 1550nm.
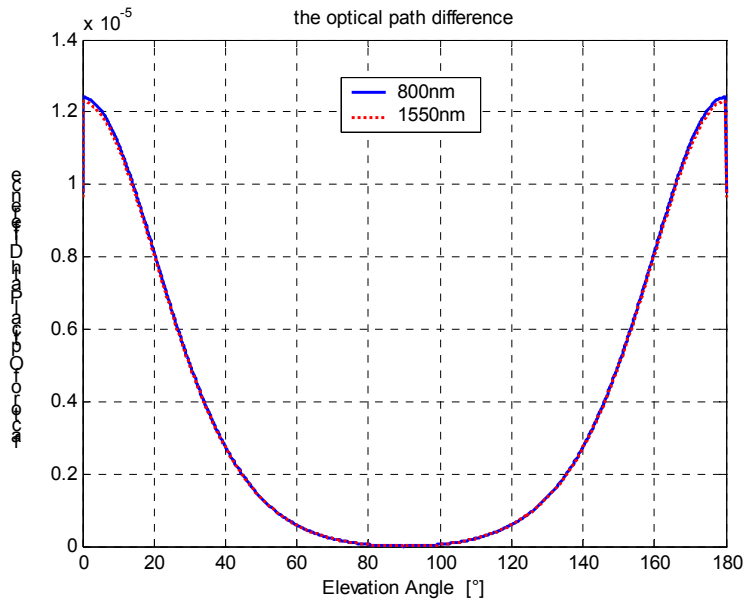
Figure 4.11 The factor of OPD for a sphere, with radius R, Mach number is M = 0.3 and air is at STP, for beams of 800nm and 1550nm

We compare the OPD of the wavelengths of 800 nm and 1550 nm. The difference between them is: $OPD_{800} = 1.009 \times OPD_{1550}$, so the difference between them is very small. From now on, we will present the results of beam with wavelength 1550 nm, with refractive index (at STP) 1.0002805.

4.5 Optical Path Difference over for a Circular Aperture

We have the same conditions as before. The flying turret is sphere, but now inside the turret there is a circular aperture. The aperture and the turret are concentric. The diameter ratio, which is the ratio of the diameters of the aperture and the turret, will fluctuate as well as the elevation angle and the free-stream Mach number. The researching area is again for radius from R until 10xR and the fluid is air. The wavelength of the beam is 1550nm.
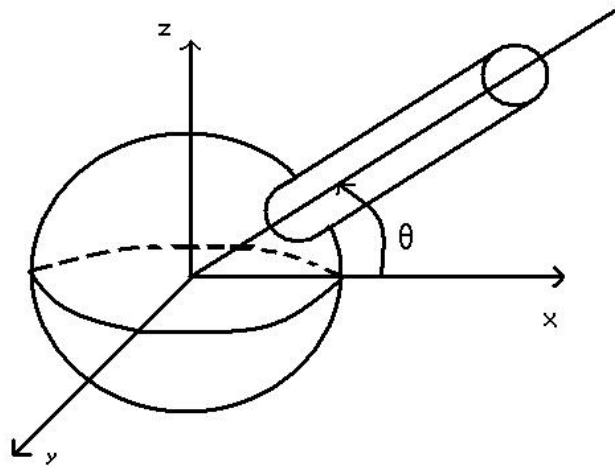
Figure 4.12   This is the propagating beam from a circular aperture in the three coordinates. We can see the boresight axis, and the elevation angle of the axis.

At the next Figures we can see the fluctuation of the wavefront for four different elevation angles, diameter ratio 1/6, Mach number 0.3 and air at STP. We see that the OPD is smaller at the angles 0° and 90° than the other two angles.
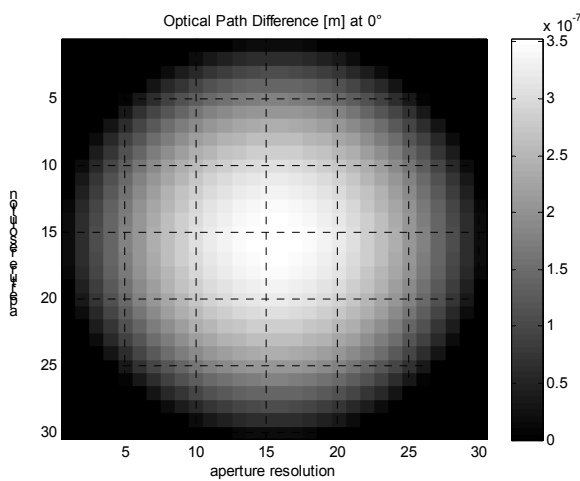
Figure 4.13 OPD at 0°
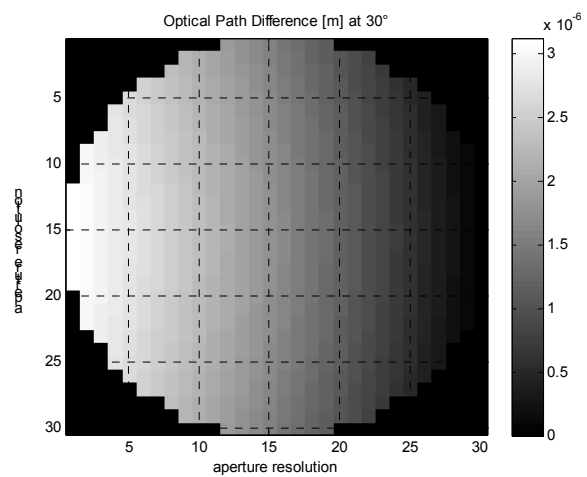
Figure 4.14 OPD at 30°
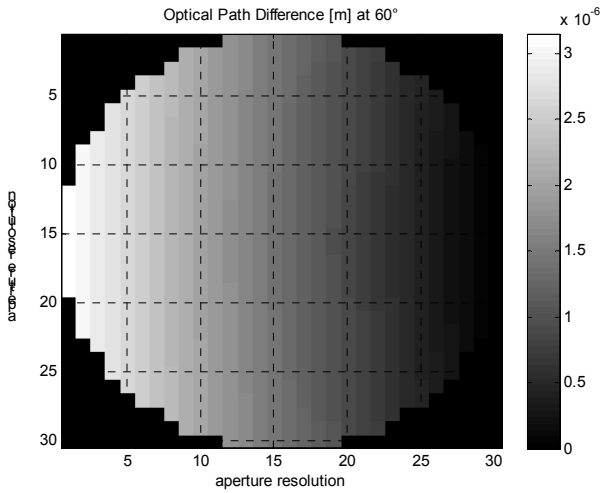
Figure 4.15 OPD at 60°
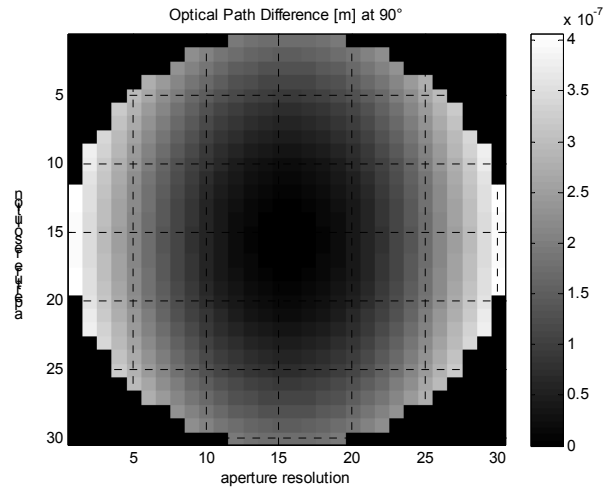
Figure 4.16 OPD at 90°

4.6 Boresight Error

Since we know the wavefront configuration, $OPD(x,y)$, we are able to calculate the boresight error, $a(x,y)$, through the wavefront phase error, $e(x,y)$: [13].

$$e(x,y) = k_0 \cdot OPD(x,y), \tag{4.11}$$

where K_0 is the wave number, and then:

$$a(x,y) = -\frac{\partial}{\partial(x,y)}\phi(x,y) = -\frac{\lambda}{2\pi} \cdot \frac{\partial}{\partial(x,y)}e(x,y) \tag{4.12}$$

We will integrate for both dimensions (x,y), Figure 4.17, of the wavefront and the results are in the next Figures (4.18 – 4.29), two for each elevation angle, one for each dimension that we integrate.
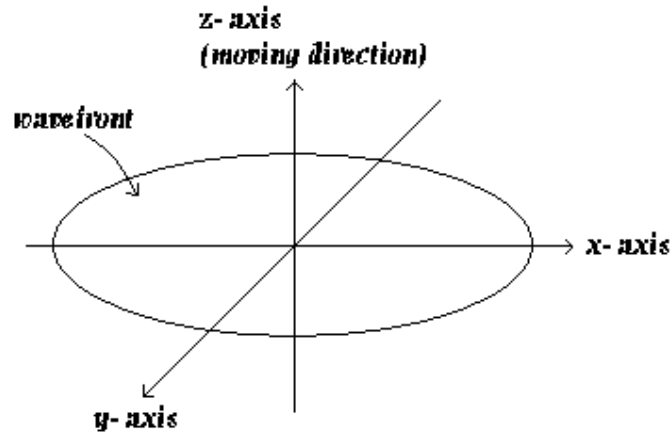
Figure 4.17 The geometry of the wavefront. In order to find the phase error of the wavefront, we have to integrate over the two dimensions (x,y).
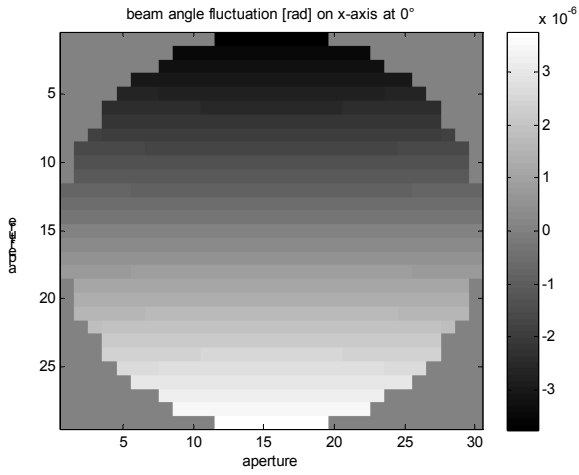
Figure 4.18 Beam aberration over x axis at 0°
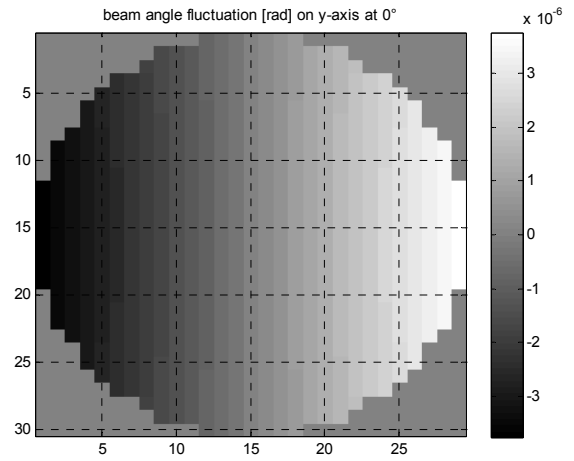
Figure 4.19 Beam aberration over y axis at 0°
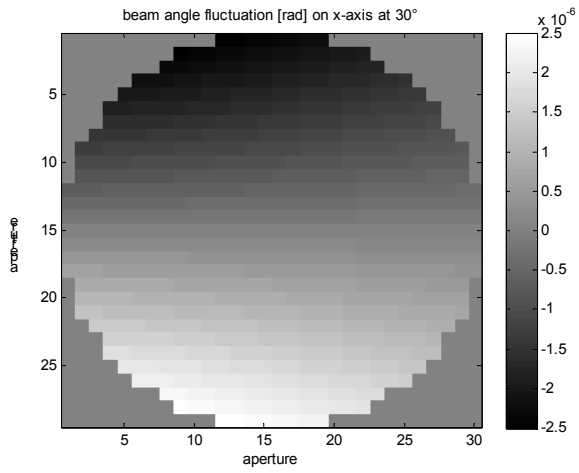
Figure 4.20 Beam aberration over x axis at 30°
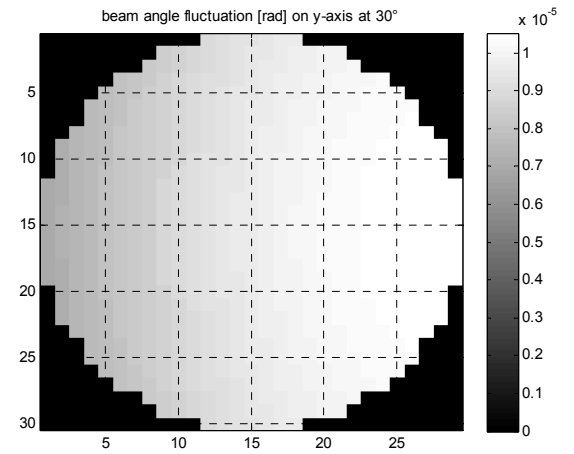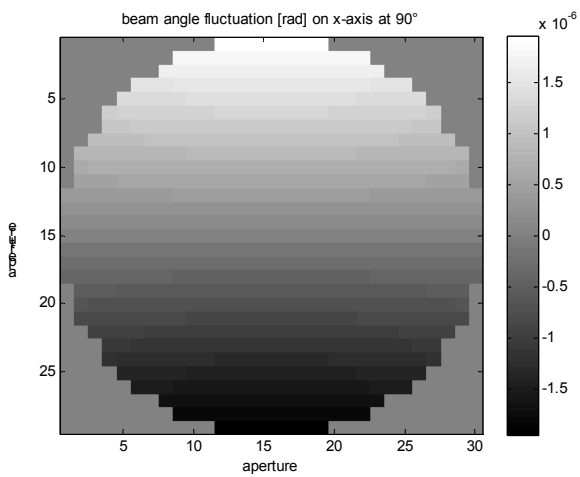

Figure 4.21 Beam aberration over y axis at 30°
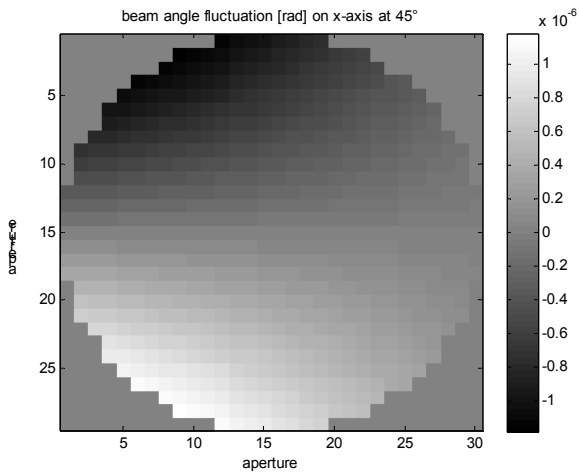
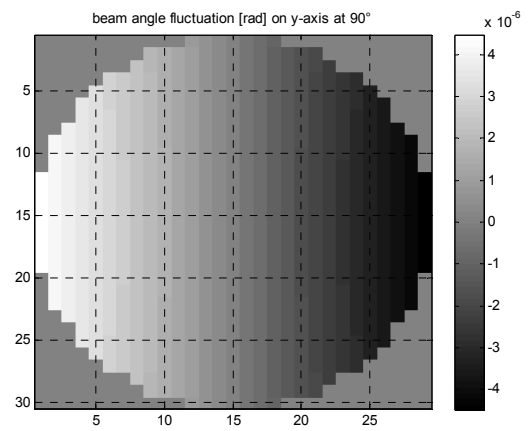**Figure 4.22** Beam aberration over x axis at 45°
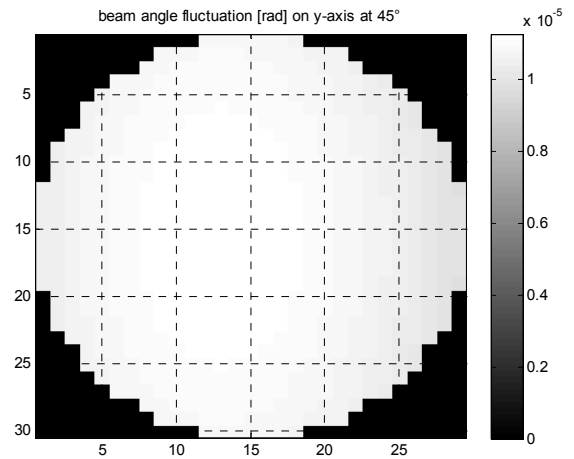
Figure 4.23 Beam aberration over y axis at 45°
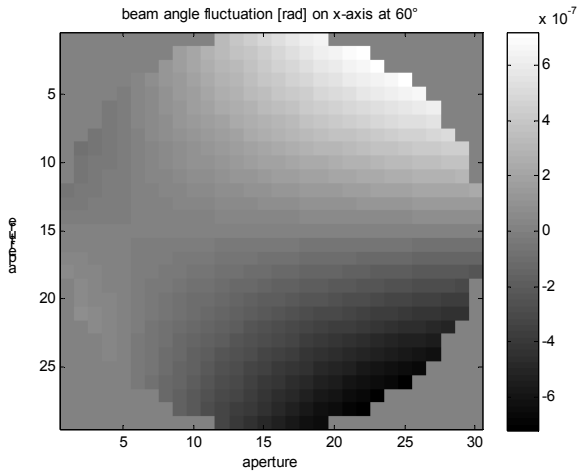
Figure 4.24 Beam aberration over x axis at 60°
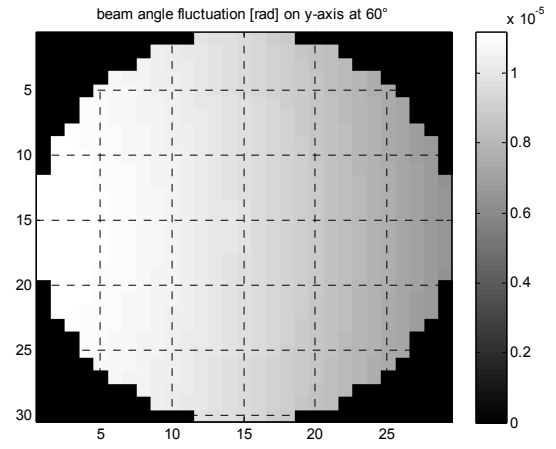
Figure 4.25 Beam aberration over y axis at 60°
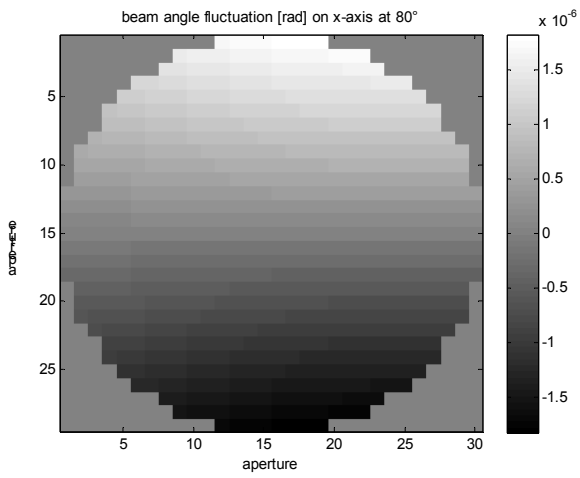
Figure 4.26 Beam aberration over x axis at 80°
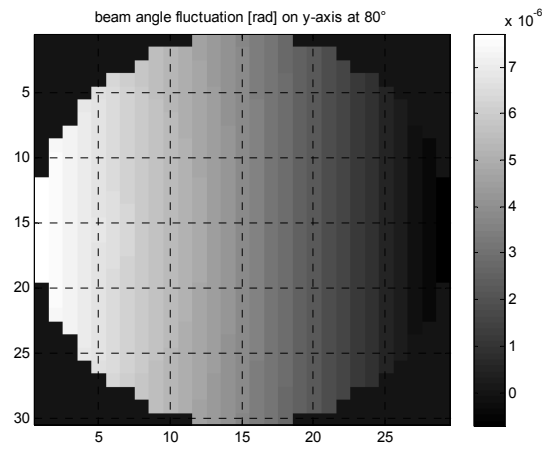
Figure 4.27 Beam aberration over y axis at 80°

Figure 4.28 Beam aberration over x axis at 90°

Figure 4.29 Beam aberration over y axis at 90°

4.7 Mean Wavefront Tilt

Knowing the boresight error, we are able to calculate the mean wavefront tilt

$$\bar{a} = \frac{1}{n} \sum_{i=n}^{n} a_i \qquad (4.13)$$

We calculate the mean tilt adding the two coordinates:

$$\bar{a} = \sqrt{\left(\bar{a}_x\right)^2 + \left(\bar{a}_y\right)^2}. \qquad (4.14)$$

4.7.1 Mean Wavefront Tilt over Elevation Angle

For the same elevation angles, with diameter ratio 1 / 6, and mach number 0.3, we can see the mean tilt of the wavefront (also for the x, y coordinates) at Table 4.1.

We see that the mean tilt over the x-axis equals for every elevation angle with 0. This means that there is symmetry over the x- axis (of the wavefront), but it happens only in this case of the spherical turret. So the mean tilt equals with the mean tilt over the y-axis of the wavefront.

elevation angle	mean angle on x- axis (μrad)	mean angle on y- axis (μrad)	mean angle (μrad)
0°	0	0	0
30°	0	9.7494	9.7494
45°	0	11.315	11.315
60°	0	9.8498	9.8498
80°	0	3.9081	3.9081
90°	0	0	0

Table 4.2 Mean wavefront tilt for several elevation angles

In Figure 4.30 there is a diagram of the mean wavefront tilt over the elevation angle. This diagram shows the mean wavefront tilt, for elevation angles at the area [0°, 90°].

We observe that the worse case – peak of the mean tilt - is for the angle at 45°, with value 11.315 μrad (table 4.1). At the angles 0° and 90° there is minimum of the mean

angle, 0 rad, although there are fluctuations. This means that there is a strong influence from the tilt angle at the mean angle of the wavefront.

In the next Figure, 4.31, we have the mean wavefront tilt over the elevation angle, for several diameter ratios. As we can see, that there is not big influence on the mean tilt, from the diameter ratio.
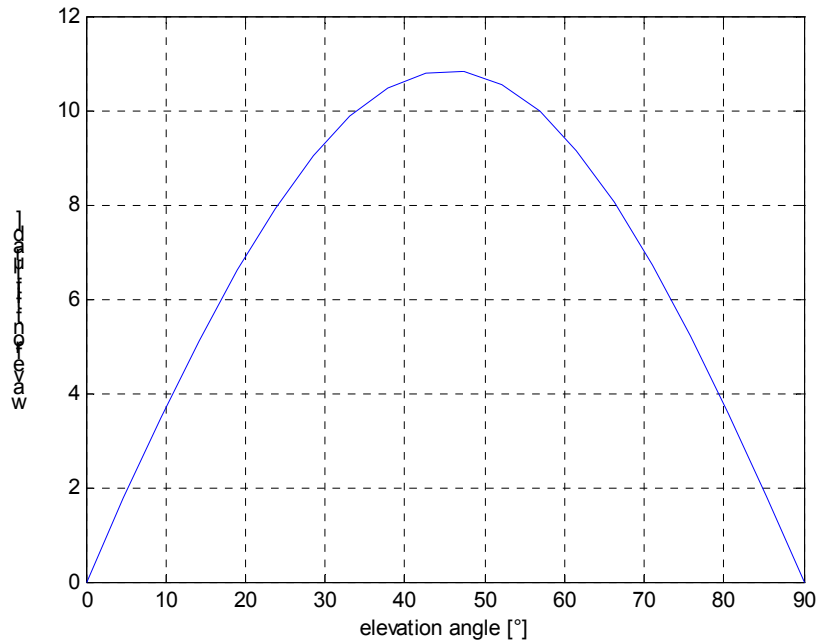

Figure 4.30 Wavefront tilt over elevation angle. d/D = 1/6, M=0.3, STP
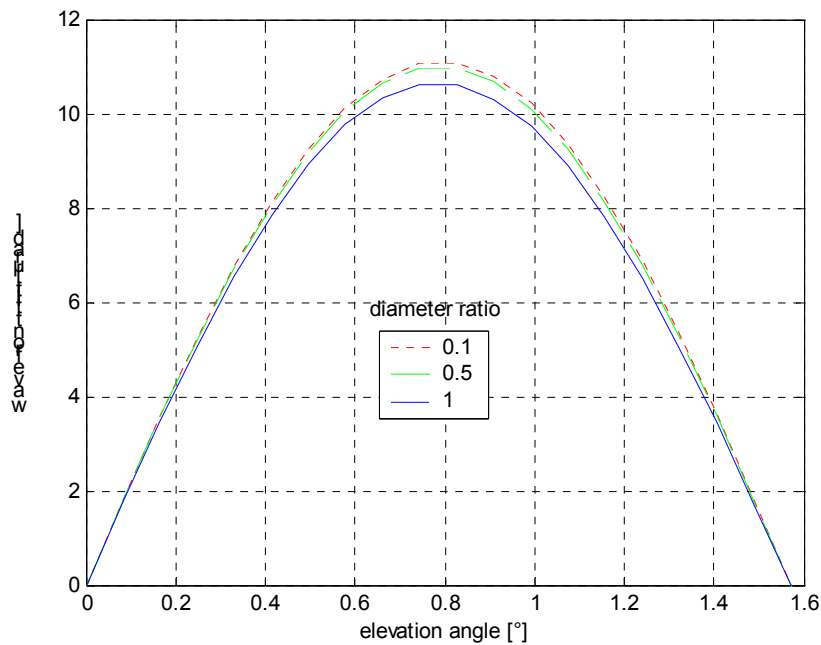

Figure 4.31 Wavefront tilt over elevation angle for several diameter ratios.
d/D = 1/6, M=0.3, STP

4.7.2 Mean Wavefront Tilt over Diameter Ratio

We investigate the mean angle of the wavefront over the aperture diameter. For the mean angle at elevation angle of 45°, we have the diagram at Figure 4.32.

We see that the fluctuation of the mean angle for ~0.5 μrad, which is small. We also observe that the biggest mean angle is when ratio is small, and is smaller when the diameter of the aperture is almost the same with the diameter of the turret.

In the next Figure, 4.33, we have the mean angle over the diameter ratio, for several elevation angles. We can compare this picture for diameter ratio 1/6, with the Figure 4.30 (from the previous paragraph), as well as do the same for the pair of Figures 4.31 and 4.32, since all of them are for the same mach number, 0.3, and air is at STP.
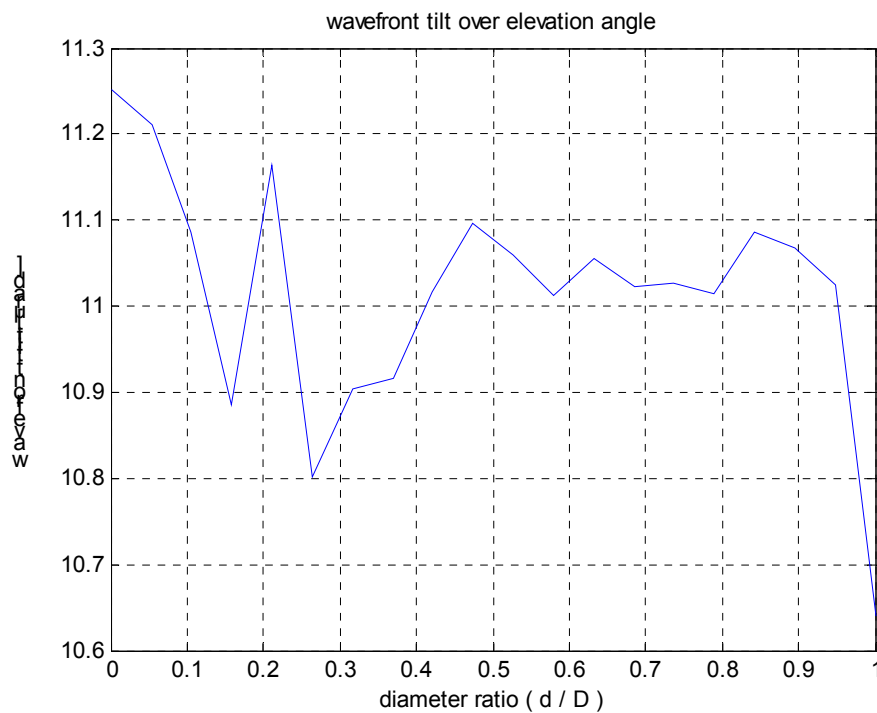
Figure 4.32 Presents the mean wavefront tilt over the diameter ratio, at 45°, M=0.3 and STP.
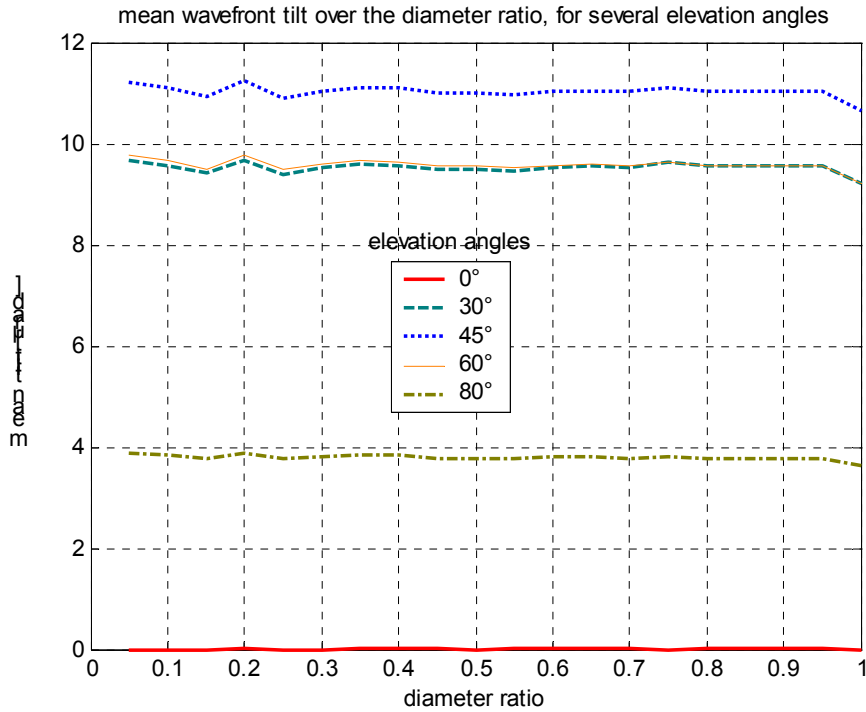
Figure 4.33 Mean wavefront tilt over diameter ratio, for several elevation angles, M=0.3, STP.

4.7.3 Mean Wavefront Tilt over Velocity

At the next Figures we will test the mean wavefront tilt over the velocity (mach number) of the flying object. Since at a compressible flow (M < 8) the perfect gas law is valid, we will have upper velocity limit this value. At STP conditions 1 Mach number equals to 331.31 m/s (Eq.2.38).
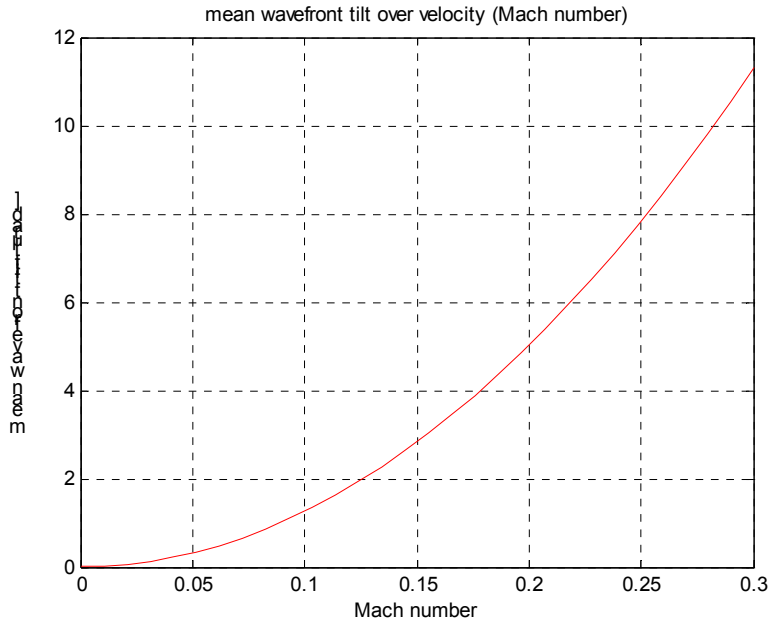
Figure 4.34 Mean wavefront tilt over Mach number, at 45°, d/D = 1/6, STP

We see that the influence of the velocity is very strong, as the Mach number is increasing.

In Figure 4.50 we see the influence of the velocity for several elevation angles, and we observe that for the higher Mach number is, the bigger tilt we have.

As far as the influence of the diameter ratio, from Fig 4.36 we see that is not very strong (as it is expected). After M = 2 there are remarkable changes, but since then there is almost no difference.
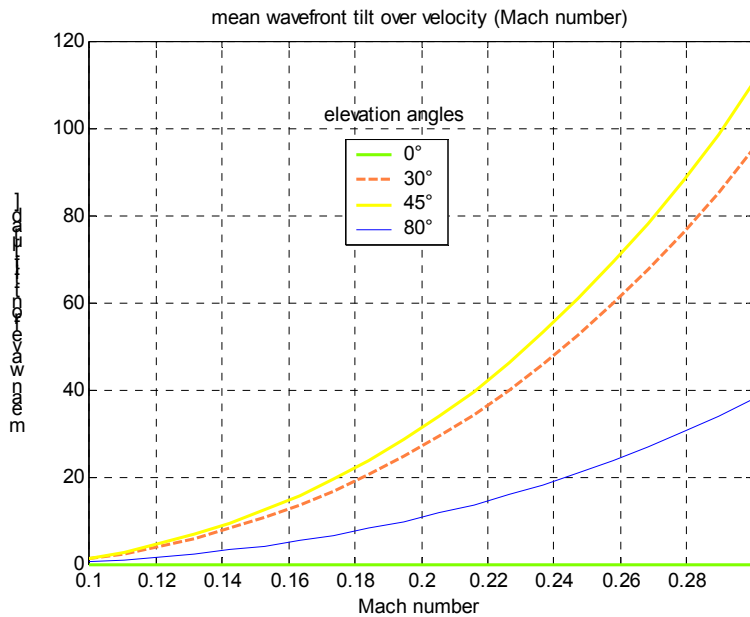
Figure 4.35 Mean tilt over Mach number, for several elevation angles, d/D = 1/6, STP
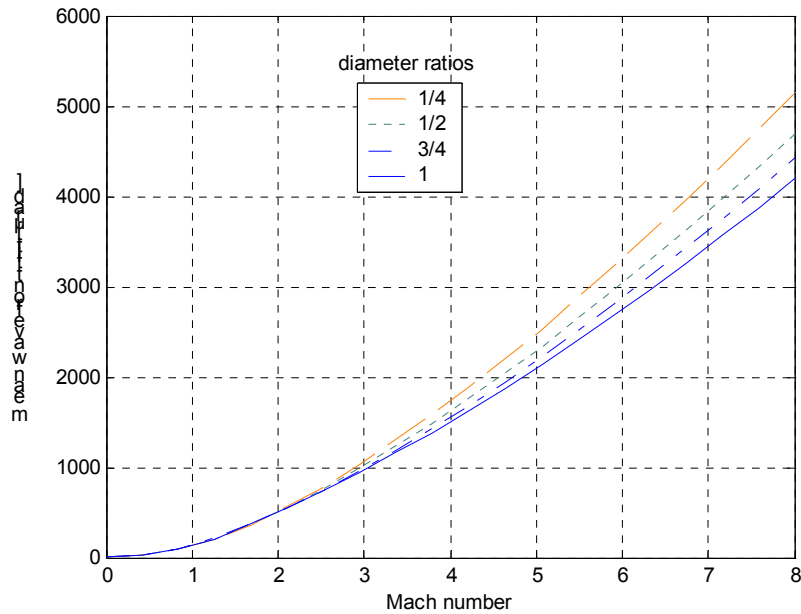
Figure 4.36 Mean tilt over Mach number for several diameter ratios, at 45°, STP

4.7.4 Mean Wavefront Tilt over Height

In §3.4 we estimated the refractive index over the altitude with three different methods. These results will we use here so that we can find the effect of the atmosphere, over the altitude, on a laser beam. This means that we have different free stream refractive index (up to here we had STP conditions, and refractive index equals with 1.0002805, for wavelength 1550 nm), which changes the refractive index around the sphere.

For further research, it is interesting to consider the type of the flying object we are going to use, the height that is going, usually, to fly and observe the mean angle at this particular height.

In Figure 4.37 we present the mean tilt of the wavefront over the height, calculated with Method A (§ 3.4.1) and the barometric formula (3.3.3). The elevation angle is 45o, the diameter ratio is 1/6 and the mach number is always 0.3. We have to take in mind that the value of the Mach number changes along the atmosphere.

In the next Figure, 4.38, we have the mean tilt over the height, for several elevation angles. We can observe the differences between the different elevation angles. This was expected from the previous results we have seen.
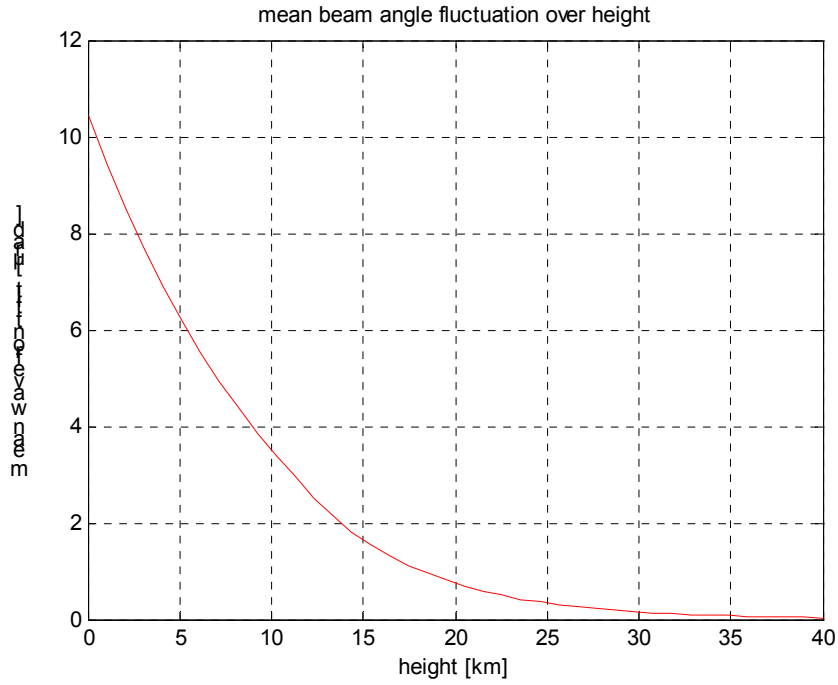
Figure 4.37 The mean tilt over the height, for several elevation angles, with method A.
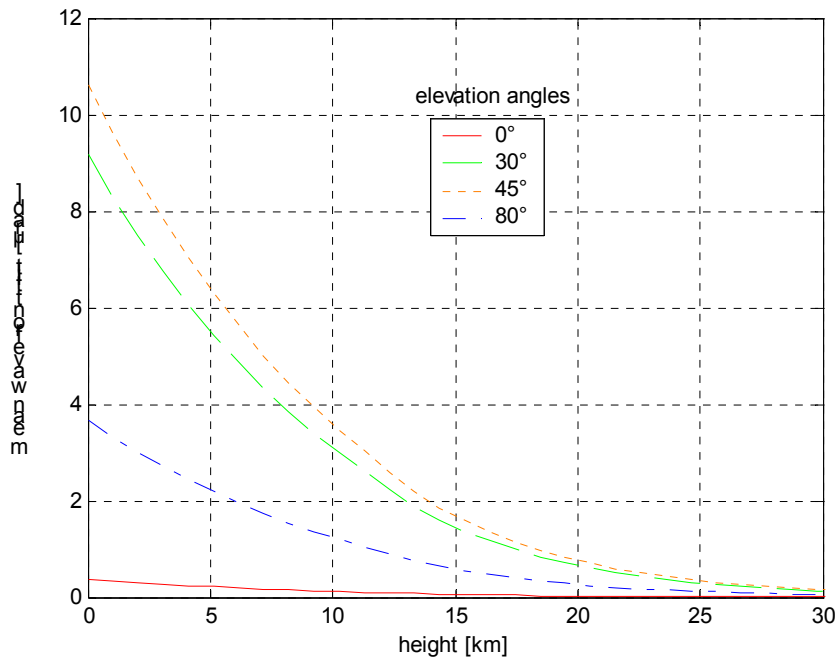elevation angle at 45°, d/D = 1/6 , M=0.3.

Figure 4.38 The mean tilt over the height, for several elevation angles, with method A, for
several elevation angles, d/D = 1/6 , M=0.3 and at STP

4.8 Zernike polynomials

An analytical measure used to characterize the fluctuation of the wavelength, are the Zernike polynomials. The 16 first Zernike polynomial functions (Z) are given at Figure 4.39. There are even and odd polynomials, which are defined, the even ones:

$$Z_n^m(\rho,\varphi) = R_n^m(\rho)\cos(m\varphi) \tag{4.15}$$

and the odd ones:

$$Z_n^{-m}(\rho,\varphi) = R_n^m(\rho)\sin(m\varphi), \tag{4.16}$$

where m and n are nonnegative integers with $n \geq m$, φ is the azimuthal angle in radians, and ρ is the normalized radial distance.

The radial polynomials R_n^m are defined as

$$R_n^m(\rho) = \sum_{k=0}^{(n-m)/2} \frac{(-1)^k (n-k)!}{k!((n+m)/2-k)!((n-m)/2-k)!} \rho^{n-2k} \tag{4.17}$$

for *n-m* even and *0* for *n-m* odd.

```
z0 = 1;                                    Piston or Bias
z1 = ρ Cos[θ];                             Tilt x
z2 = ρ Sin[θ];                             Tilt y
z3 = -1 + 2 ρ²;                            Power
z4 = ρ² Cos[2 θ];                          Astig x
z5 = ρ² Sin[2 θ];                          Astig y
z6 = ρ (-2 + 3 ρ²) Cos[θ];                 Coma x
z7 = ρ (-2 + 3 ρ²) Sin[θ];                 Coma y
z8 = 1 - 6 ρ² + 6 ρ⁴;                      Primary Spherical
z9 = ρ³ Cos[3 θ];                          Trefoil x
z10 = ρ³ Sin[3 θ];                         Trefoil y
z11 = ρ² (-3 + 4 ρ²) Cos[2 θ];            Secondary Astigmatism x
z12 = ρ² (-3 + 4 ρ²) Sin[2 θ];            Secondary Astigmatism y
z13 = ρ (3 - 12 ρ² + 10 ρ⁴) Cos[θ];       Secondary Coma x
z14 = ρ (3 - 12 ρ² + 10 ρ⁴) Sin[θ];       Secondary Coma y
z15 = -1 + 12 ρ² - 30 ρ⁴ + 20 ρ⁶;         Secondary Spherical
```

Figure 4.39 The equations and the names for the 16 first Zernike Polynomials [14]

The equation for the wavefront (ϕ) as a function of the Zernike Polynomials is

$$\phi(x, y, z) = \sum_{j=1}^{N} A_j Z_j \qquad (4.18)$$

where A_j is the Zernike coefficient, defined as:

$$A_j = \int_0^{2\pi} \int_0^R \phi_j(r, \theta) \cdot Z_j(r, \theta) \cdot r \cdot dr \cdot d\theta \,. \qquad (4.19)$$

The Zernike coefficients show us the effect of the corresponding Zernike polynomial at the wavefront.

The first six Zernike polynomials are presented at Figures 4.40 – 4.45. At the next six Figures (Figures 4.46 – 4.51) are presented the variation of the 6 first coefficients (each one for the corresponding polynomial) for elevation angles from 0° to 90°. We observe that the 1st coefficient (piston) does not have any consequences at the wavefront fluctuations, since it is flat. Comparing the familiar polynomials (tilt, astigmatism) we see that there is bigger tilt over the x-axis than the y-axis, but the astigmatism is more over the y-axis than the x-axis. We also have focus or defocus problem (when the coefficient is positive or negative). But we have to be careful, that this is not the mean tilt of the wavefront, which will be presented in the next paragraphs. At Figures 4.52 – 4.58 are we can see the effect of each coefficient for 6 elevation angles, (0°, 30°, 45°, 60°, 80°, 90°).
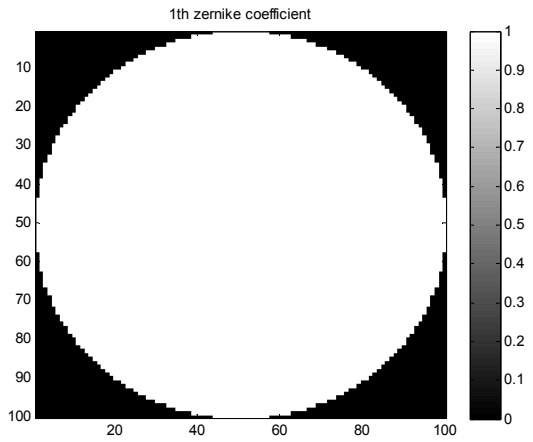
Figure 4.40 the 1st Zernike polynomial: Piston
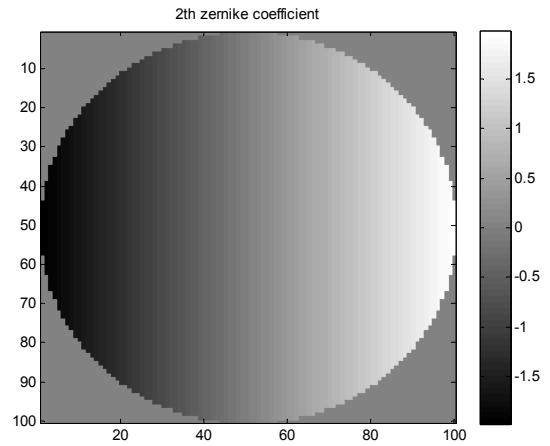
Figure 4.41 the 2nd Zernike polynomial: Tilt on x-axis
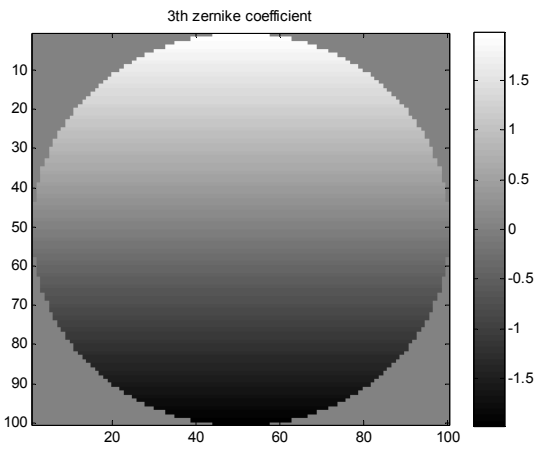
Figure 4.42 the 3rd Zernike polynomial:
Tilt on y-axis
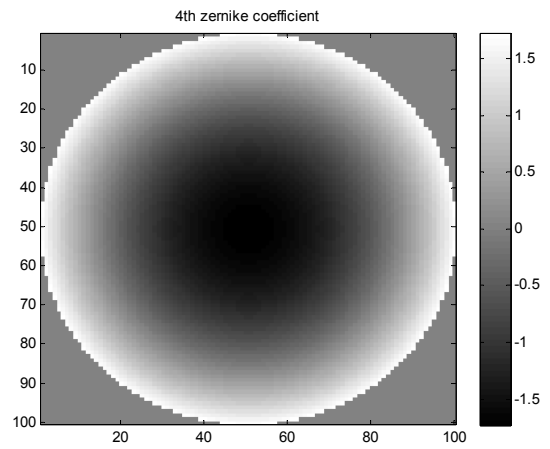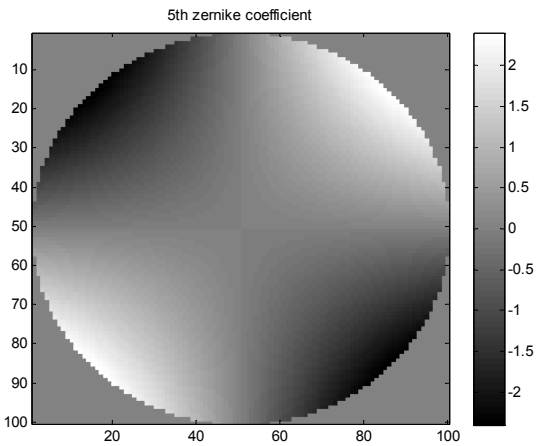

Figure 4.43 the 4th Zernike polynomial:
Focus

Figure 4.44 the 5th Zernike polynomial:
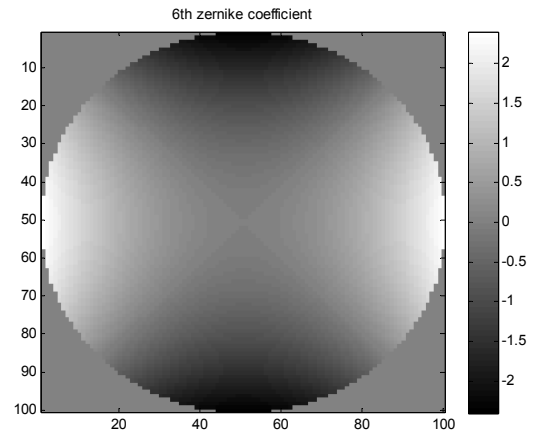Astigmatism on x-axis

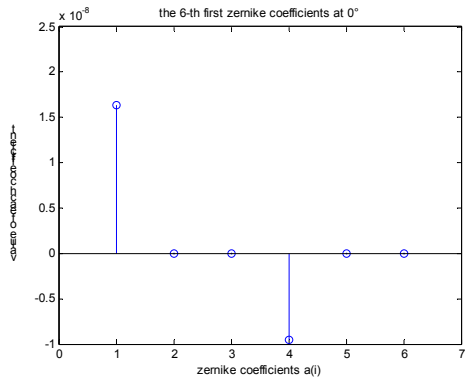**Figure 4.45** the 6th Zernike polynomial:
Astigmatism on y-axis

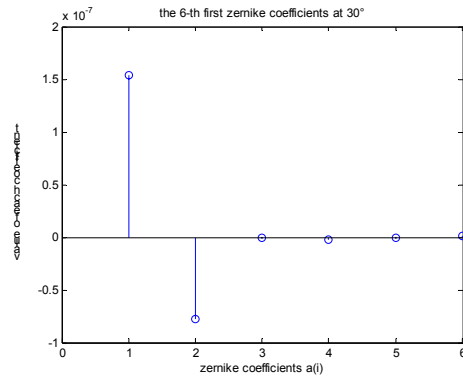**Figure 4.46** the first 6 Zernike polynomials at 0°
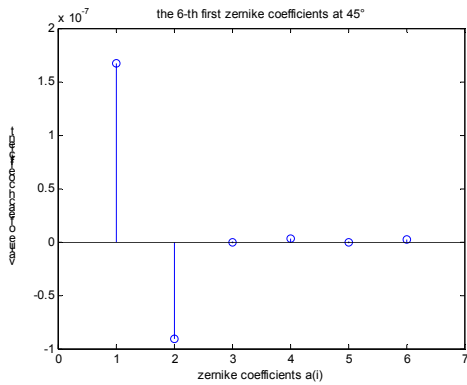

Figure 4.47 the first 6 Zernike polynomials at 30°

Figure 4.48 the first 6 Zernike polynomials at 45°
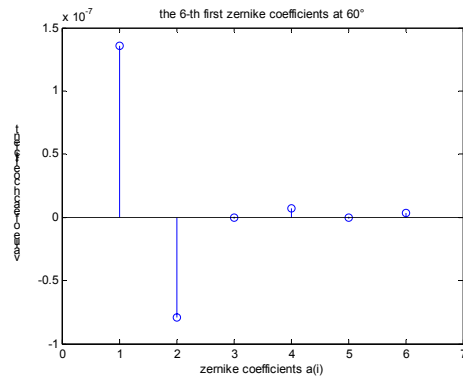
Figure 4.49 the first 6 Zernike polynomials at 60°
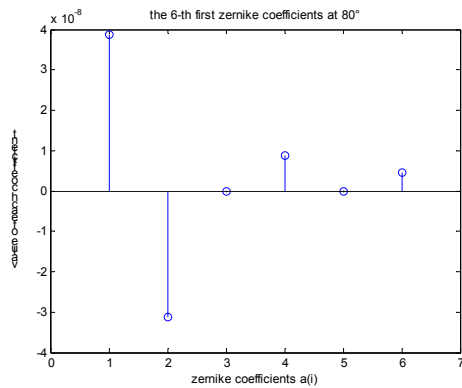
Figure 4.50 the first 6 Zernike polynomials at 80°
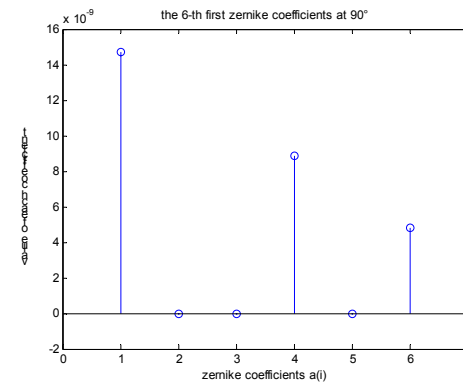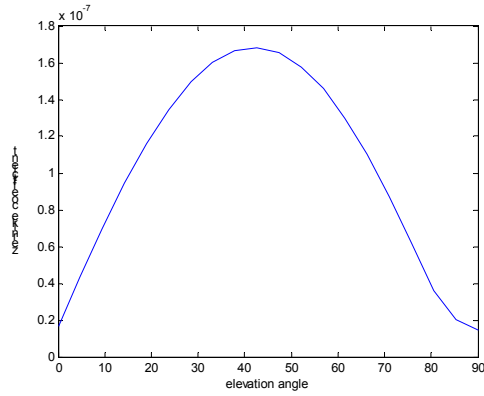

Figure 4.51 the first 6 Zernike polynomials at 90°

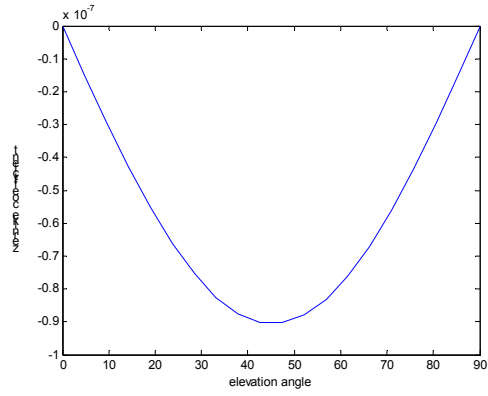**Figure 4.52** the 1st Zernike polynomial: Piston, over elevation angle. d/D = 1/6, M=0.3, STP

Figure 4.53 the 2nd Zernike polynomial: Tilt on x-axis, over elevation angle. d/D = 1/6, M=0.3, STP
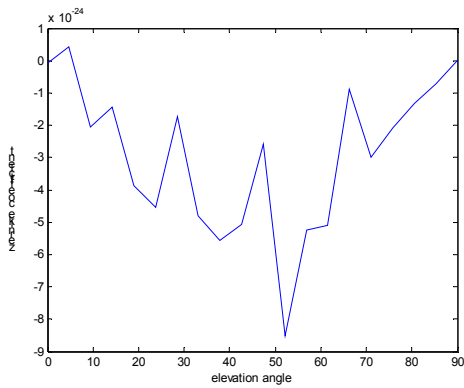

Figure 4.54 the 3rd Zernike polynomial: Tilt on y-axis, over elevation angle. d/D = 1/6, M=0.3, STP
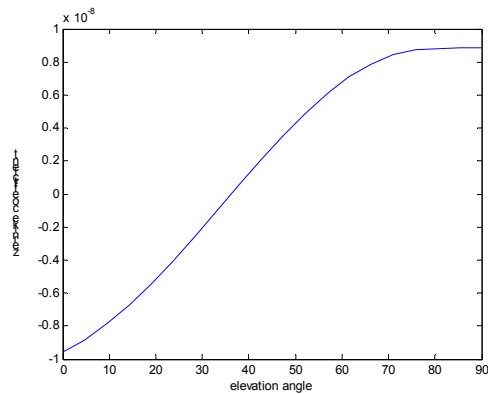

Figure 4.55 the 4th Zernike polynomial: Focus, over elevation angle. d/D = 1/6, M=0.3, STP
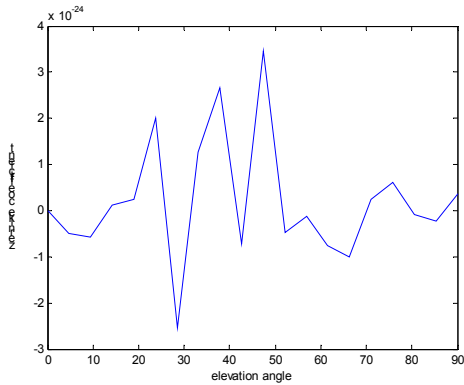

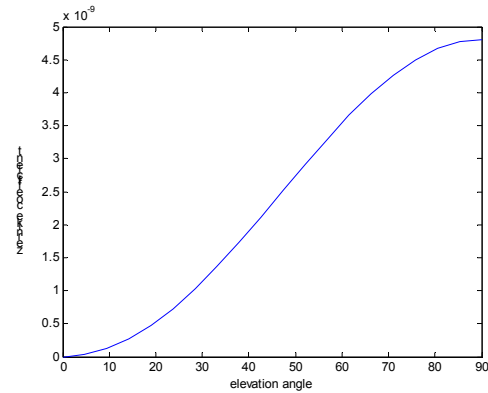**Figure 4.56** the 5th Zernike polynomial: Astigmatism on x-axis, over elevation angle. d/D = 1/6, M=0.3, STP

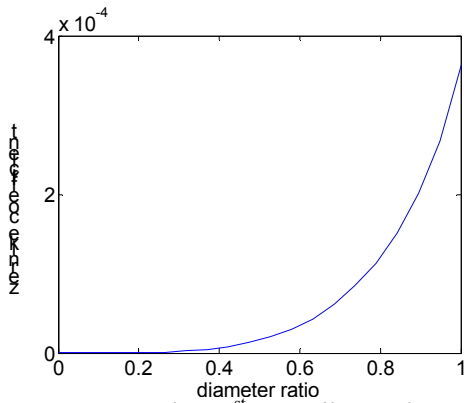**Figure 4.57** the 6th Zernike polynomial: Astigmatism on y-axis, over elevation angle. d/D = 1/6, M=0.3, STP

Figure 4.58 the 1st Zernike polynomial: Piston, over diameter ratio. Elevation angle is 45°, M=0.3, STP
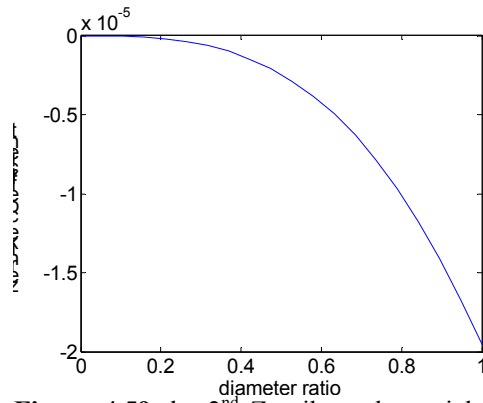

Figure 4.59 the 2nd Zernike polynomial: Tilt on x-axis, over diameter ratio. Elevation angle is 45°, M=0.3, STP
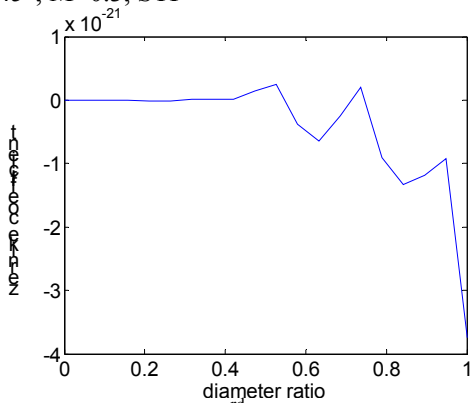

Figure 4.60 the 3rd Zernike polynomial: Tilt on y-axis, over diameter ratio. Elevation angle is 45°, M=0.3, STP
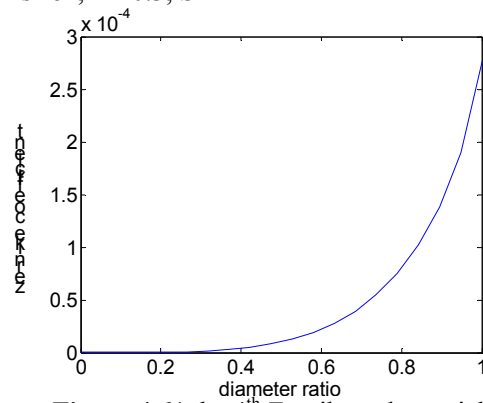

Figure 4.61 the 4th Zernike polynomial: Focus, over diameter ratio. Elevation angle is 45°, M=0.3, STP
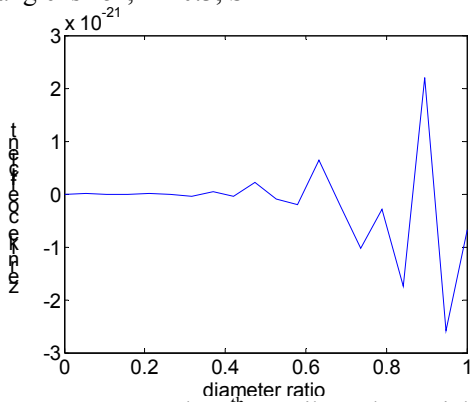

Figure 4.62 the 5th Zernike polynomial: Astigmatism on x-axis, over diameter ratio. Elevation angle is 45°, M=0.3, STP
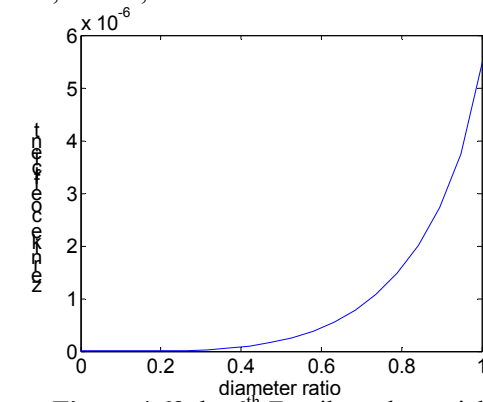

Figure 4.63 the 6th Zernike polynomial: Astigmatism on y-axis, over diameter ratio. Elevation angle is 45°, M=0.3, STP
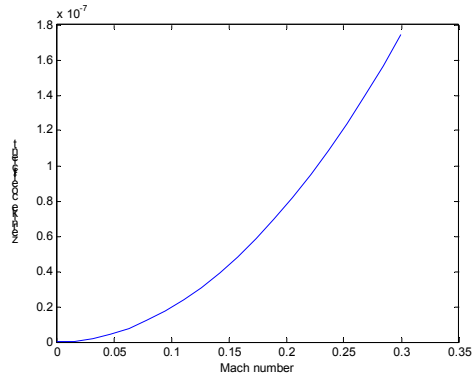
Figure 4.64 the 1st Zernike polynomial: Piston, over velocity. Elevation angle is 45°, d/D = 1/6, STP

Figure 4.65 the 2nd Zernike polynomial: Tilt on x-axis, over velocity. Elevation angle is 45°, d/D = 1/6, STP

Figure 4.66 the 3rd Zernike polynomial: Tilt on y-axis, over velocity. Elevation angle is 45°, d/D = 1/6, STP

Figure 4.67 the 4th Zernike polynomial: Focus, over velocity. Elevation angle is 45°, d/D = 1/6, STP

Figure 4.68 the 5th Zernike polynomial: Astigmatism on x-axis, over velocity. Elevation angle is 45°, d/D = 1/6, STP

Figure 4.69 the 6th Zernike polynomial: Astigmatism on y-axis, over velocity. Elevation angle is 45°, d/D = 1/6, STP
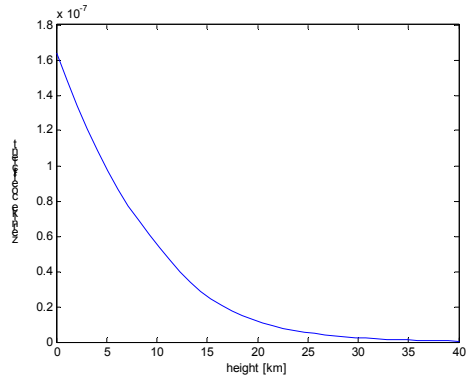
Figure 4.70 the 1st Zernike polynomial: Piston, over height. Elevation angle is 45°, d/D = 1/6, M=0.3
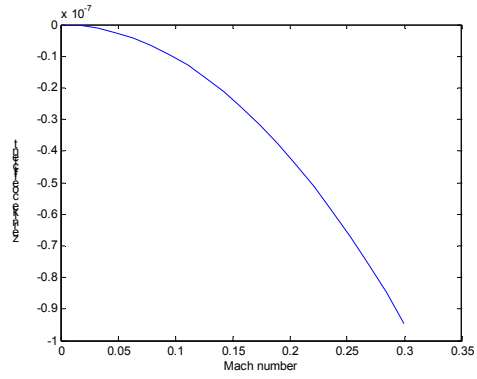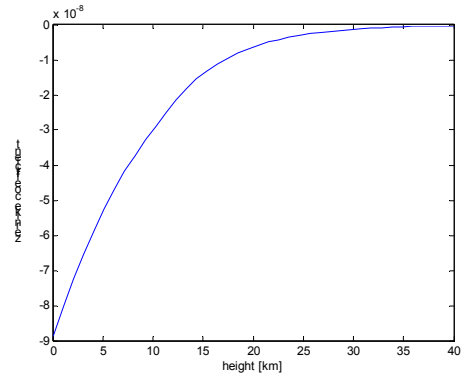

Figure 4.71 the 2nd Zernike polynomial: Tilt on x-axis, over height. Elevation angle is 45°, d/D = 1/6, M=0.3
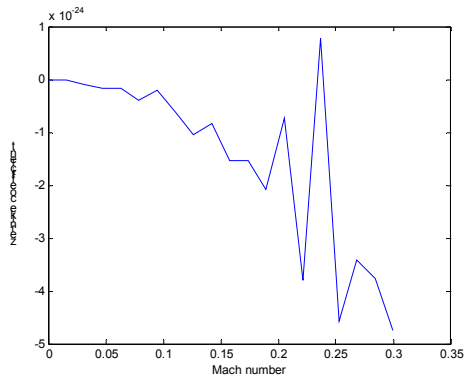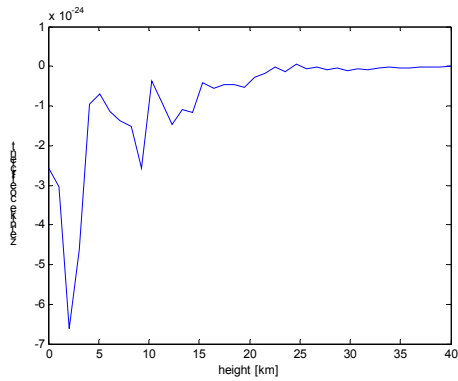

Figure 4.72 the 3rd Zernike polynomial: Tilt on y-axis, over height. Elevation angle is 45°, d/D = 1/6, M=0.3
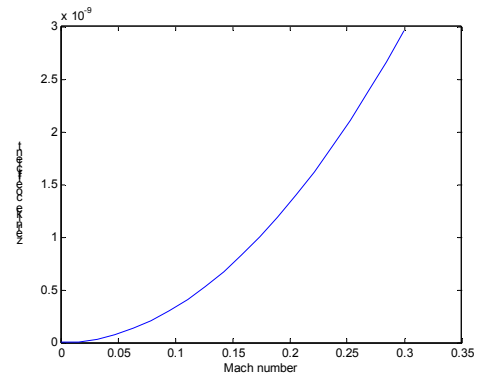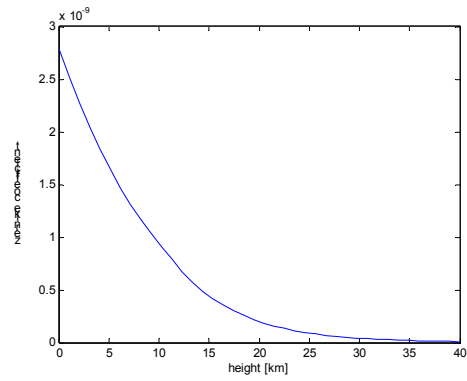

Figure 4.73 the 4th Zernike polynomial: Focus, over height. Elevation angle is 45°, d/D = 1/6, M=0.3
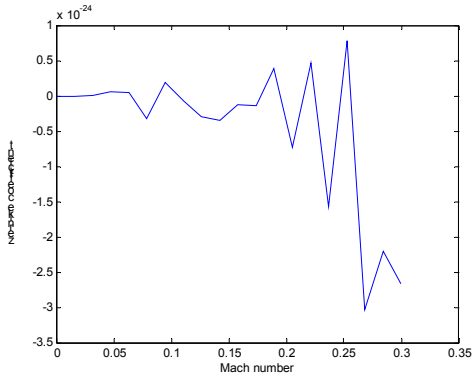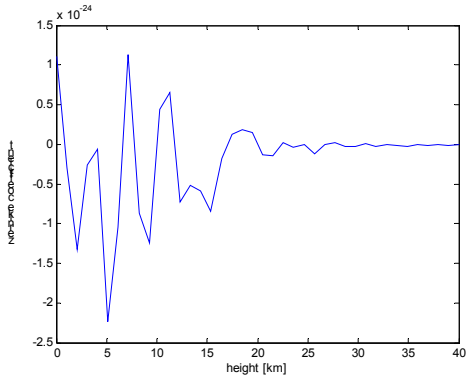

Figure 4.74 the 5th Zernike polynomial: Astigmatism on x-axis, over height. Elevation angle is 45°, d/D = 1/6, M=0.3
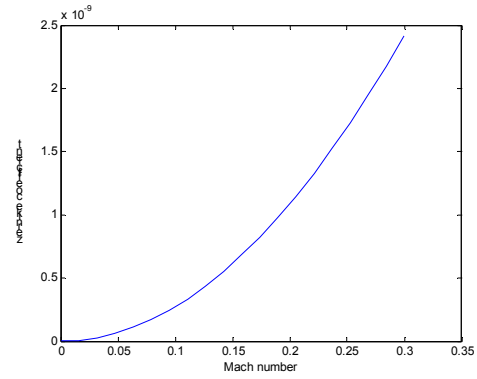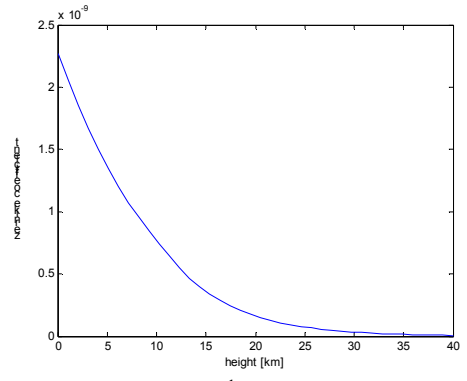

Figure 4.75 the 6th Zernike polynomial: Astigmatism on y-axis, over height. Elevation angle is 45°, d/D = 1/6, M=0.3

4.9 Root Mean Square OPD

Another variable we can research to define the wavefront fluctuations is the difference-Root Mean Square (RMS) of the wavefront, defined as:

$$OPD_{RMS} = \frac{1}{S}\sqrt{\int\left(OPD^2 - \overline{OPD}^2\right)dx \cdot dy} \; , \qquad (4.20)$$

where S is the surface of the aperture.

At the next Figure, 4.76, we can observe the OPD_{RMS} over the elevation angle. In Figure 4.73 we have a diagram for the OPD_{RMS} over the diameter ratio and we see that the influence is very strong, something that was expected. The next two Figures (4.74, 4.75) depict the OPD_{RMS} over the velocity, and over the height.
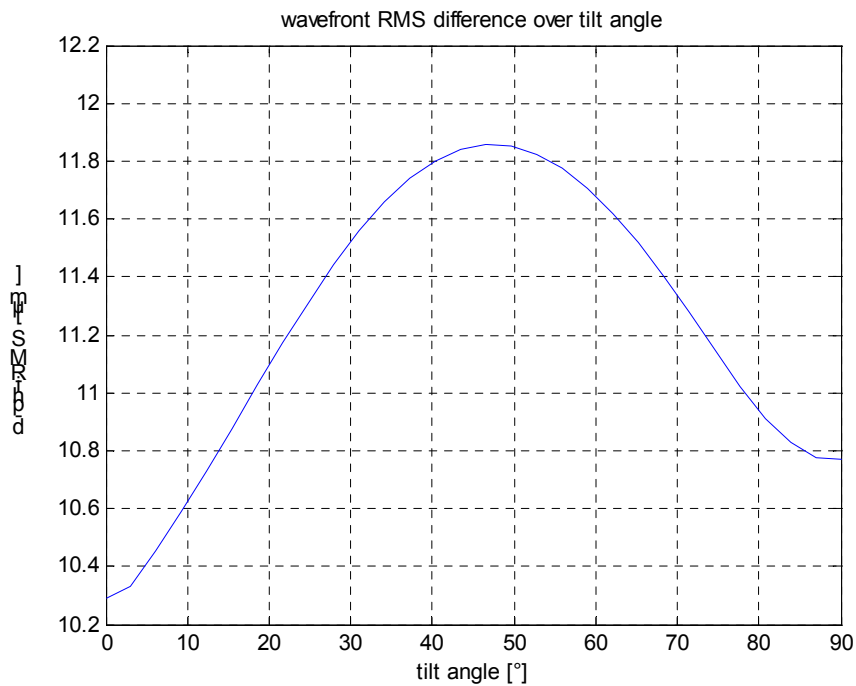
Figure 4.76 The OPD_{RMS} over the elevation angle. Diameter ratio is 1/6, M = 0.3 and air at STP
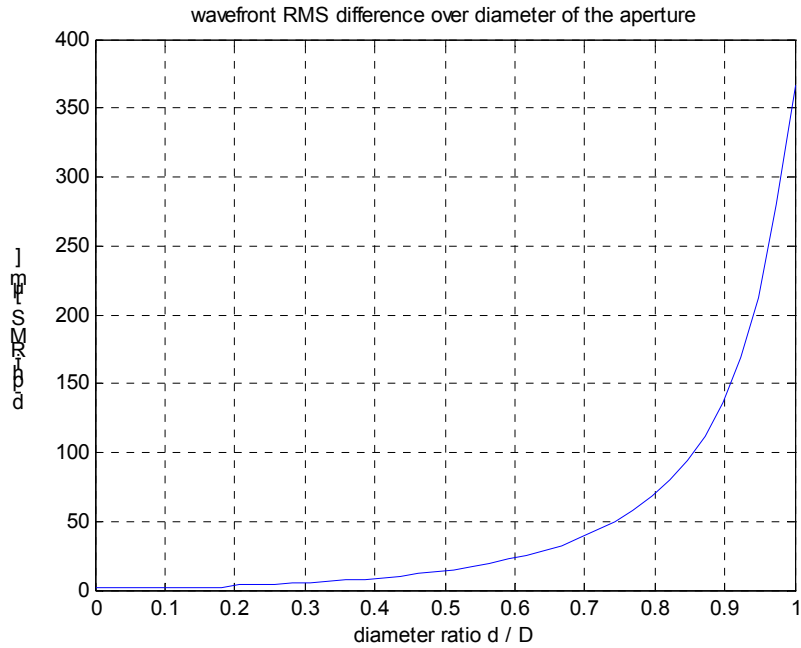
Figure 4.77 The OPD_{RMS} over the diameter ratio of the aperture and the turret. Elevation angle is 45°, M = 0.3 and air at STP.
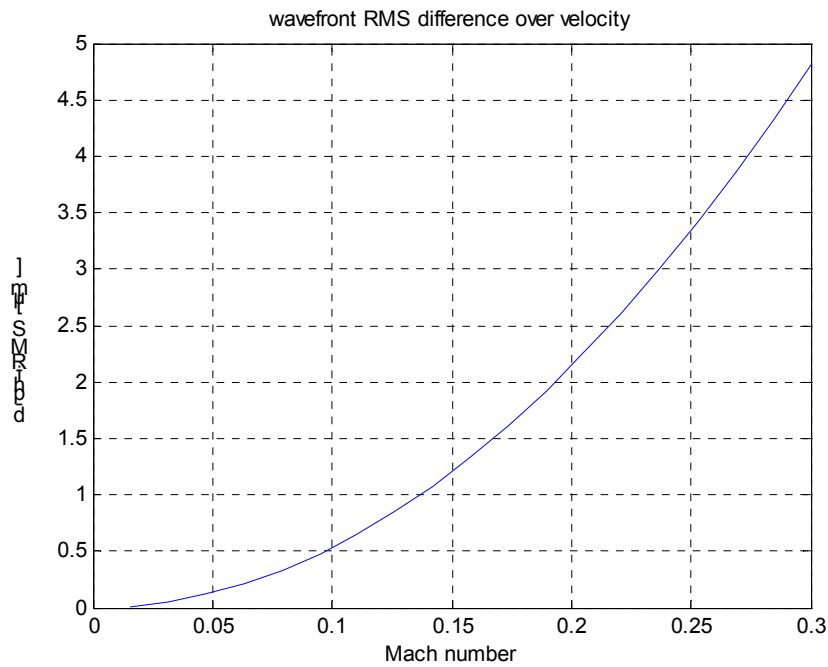
Figure 4.78 The OPD_{RMS} over the velocity. Elevation angle is 45°, diameter ratio 1/6 and air at STP.
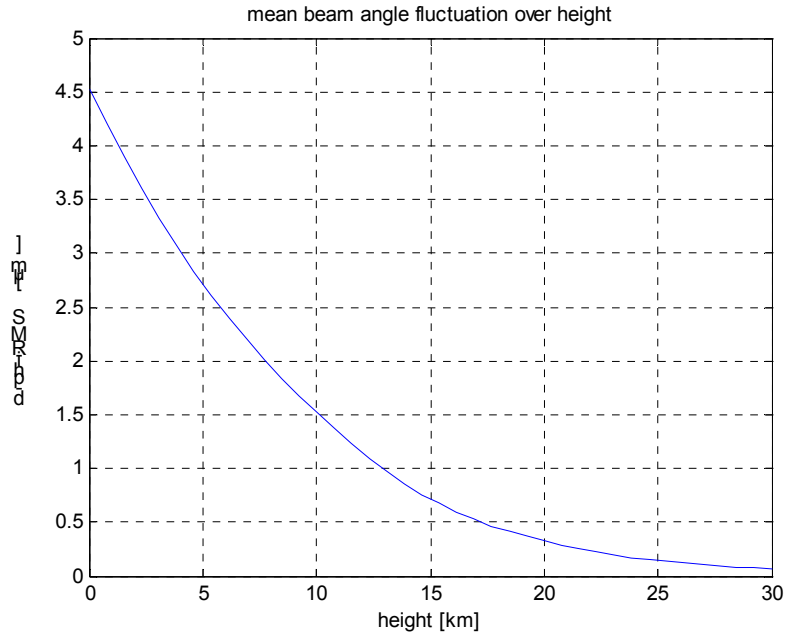
Figure 4.79 The OPD_{RMS} over the height. Elevation angle is 45°, diameter ratio 1/6 and M = 0.3.

5

Conclusion

5.1 Results

In this thesis we have seen the distortions of the flow-field on a laser beam. We have firstly defined one case of flow around the turret, described the flow with equations and then applied a method to describe the wavefront distortions of the beam.

We see that the flow around the sphere is symmetrical (pressure and velocity). This is because we assume potential flow. This case leads us to the d'Alembert's Paradox - Jean Le Rond d'Alembert (1717-1783). The paradox says that on an object moving in a potential field there is no drag. But experiments showed other results.

The answer was given almost 200 years later, in 1904, from Ludwig Prandtl, who introduced the boundary layer theory. This theory says that the drag is created from the boundary layers (§ 2.6), created on the surface of the object. The equations that we have used (and d'Alembert used) are not able to "understand" the boundary layers at this kind of flow. As we have seen at Figures 4.3, 4.4 these kind of flow is limited, since the diameter of the sphere should be very small in order to have steady, incompressible flow (Re<40).

Although, we get the first idea, how the flow impacts the laser beam from or to the object. If we find the other types of flow, and calculate the velocity around an object, then we can apply this method on a laser beam and calculate the distortions due to this flow.

We can see how each parameter effects the distortions. The parameters are the elevation angle, the diameter of the aperture (the diameter of the turret for a sphere has no influence at the flow, but only in the case of a sphere – but of course is has consequences at the value of the Reynolds number), and as well as the free-stream velocity and the height that the object is. For this reason we usually consider the worse cases (e.g. elevation angle = 45$^{\mathrm{o}}$, M = 0.3).

Changing the previous parameters, we have bigger Reynolds numbers, where there is separation of the boundary layers, so there is weak (Figure 4.1). As far as the flow is laminar, experimental results show that the flow is very similar, up to the separation point. The same happens for other turret geometries such as hemispheres. These fields (different conditions and different shape) are going to be the next researching steps in this topic (Figures 4.80 - 4.81).

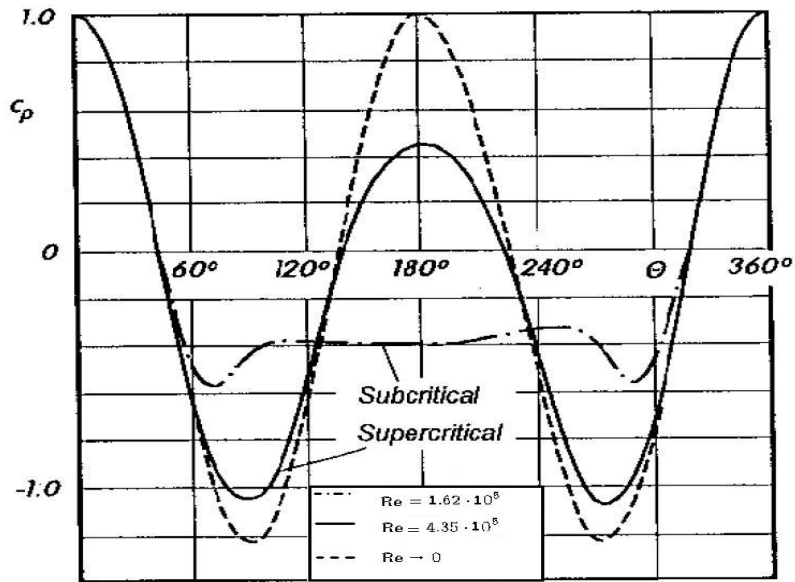**Figure 5.1** The pressure coefficient after measurements by O. Flashboard around a sphere for several Reynolds number. We have to mention that the values of the Reynolds numbers (except the case that Re → 0) are very high: 162000 and 435000 (turbulent flow). [1]
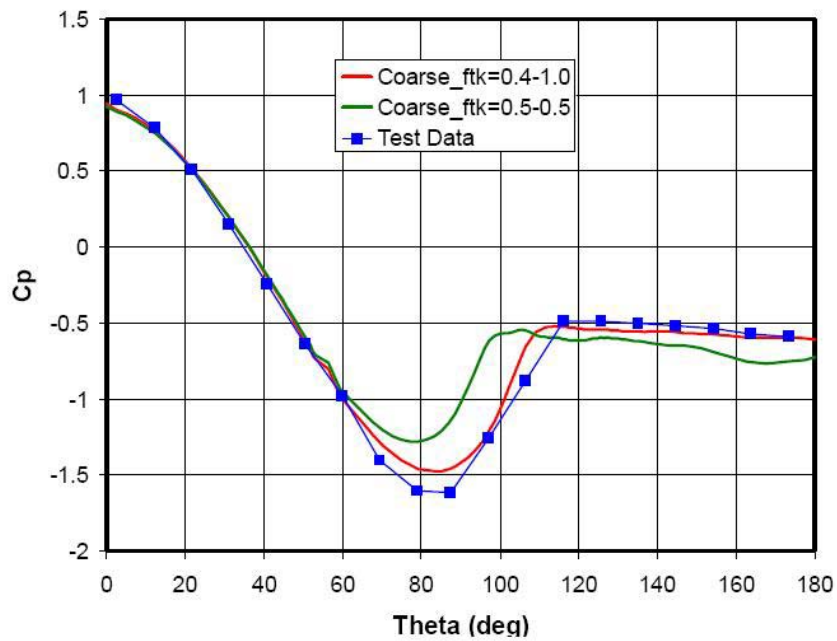

Figure 5.2 The pressure coefficient after measurements and CFD-results (Computational Fluid Dynamics) over the elevation angle.[15]

5.2 Further Research

As we mentioned in the previous paragraph, there is a lot of things to research more in this topic. Firstly we have to focus on other turret shapes, such as hemisphere, thinking a hemisphere turret. The turret will be on an aircraft. So we have to research the shapes of the aircrafts and their wings. They are mostly described from the airfoils. The final goal is to simulate the flow field around an aircraft with a turret on it. In this case we will have the "real - shape" simulation. Then we can decide where is the best place on the aircraft to put the turret, with an antenna inside.

After the different shapes we can study different flows, in different flow conditions. This leads to the increase of the Reynolds number, and from laminar to turbulent flow. It would be very interesting to study all the types of flow, which include also boundary layers, and end up to the turbulent flow (Figure 4.2). The last one is a great challenge for all the mathematicians and physicists, since the description and the understanding of the turbulent flow is one of the biggest mathematic problems these days. If we reach this level, we can simulate the "real - condition" flow.

Adding these two branches of the research, we will have the "real" simulation of a flying aircraft. Then if we apply our method for the laser beam distortions we will know the impact of the boundary layer on the laser beam propagation.

We see that in this field of research there is not only CFD. For this reason we can also study on the method that calculates the distortions. We have already showed one, but we can always improve this method and find new ways to describe the wavefront distortions.

Symbols

Symbol	Nomenclature	Units (SI)
a	boresight error	rad
A_j	Zernike coefficient	-
b	height stage	m
c	speed of light	m/s
c_p	heat capacity at constant pressure	kg
C_p	pressure coefficient	-
c_v	heat capacity at constant volume	kg
d	diameter of the aperture	m
D	diameter of the sphere	m
e	phase error	-
f	forces	N
G	Gladstone-Dale constant	-
h	geopotential height	m
k_o	wave number	m^{-1}
L_c	characteristic length	m
L_b	temperature lapse rate	k/m
L	distance of research	m
M	mach number	-
Moll	molecule mass	kg
n	refractive index	-
n_d	differential refractive index	-
OPD	optical path difference	m
OPL	optical path length	m
p	pressure	pascal
P_t	total pressure	pascal
R_{gas}	gas constant	J/(mol x k)
R	radius of the sphere	m
r	length of the beam	m
$\overline{R}$	special gas constant	J/(kg x k)
R_n^m	radial polynomial	-
Re	Reynolds number	-
T	temperature	K, ^{o}C
t	time	s
U	velocity	m/s
u	velocity coordinate over x- axis	m/s

Symbol	Nomenclature	Units
v	velocity coordinate over y- axis	m/s
V	volume	m^3
w	velocity coordinate over z- axis	m/s
x	x- axis	-
y	y- axis	-
z	z- axis	-
Z_j	Zernike polynomial	-
α	speed of air	m/s
γ	adiabatic index	-
θ	elevation angle	^{o}
λ	wavelength	m
μ	viscosity	pascal x s
ρ	density	kg/m^3
τ	shear stress	pascal
φ	velocity field	m/s^2
ω	vorticity	-

Abbreviations

CFD   Computational Fluid Dynamics

DLR   Deutsches Zentrum fur Luft- und Raumfahrt

EADS   European Aeronautic Defence and Space Company

ICAO   International Civil Aviation Organization

ISA   International Standard Atmosphere

LOLA   Liaison Optique Laser Aeroportee

NASA   National Aeronautics and Space Administration

NTUA   National Technical University of Athens

OPD   Optical Path Difference

OPL   Optical Path Length

RMS   Root Mean Square (see: OPD_{RMS})

STP   Standard Temperature and Pressure

UAV   Unman Aircraft Vehicle

References

[1]   H. Schlichting, K. Gersten: Boundary Layer Theory

[2]   D.J. Tritton: Physical Fluid Dynamics

[3]   http://www.grc.nasa.gov/

[4]   K.G. Gilbert, L.J. Otten, W.C. Rose, IR/EO Handbook, chapter 3: Aerodynamic   Effects

[5]   http://pds-atmospheres.nmsu.edu/

[6]   E. Carafoli: Wing Theory in Supersonic Flow, 1969

[7]   J. Seddon, E.L. Goldsmith: Intake Aerodynamics

[8]   G. Havener, Optical Wave Front Variance: A study on Analytic Models in Use Today, 1992, AIAA 992-0654

[9]   M.I. Jones, E.E. Bender: CFD – Based Computer Simulation of Optical Turbulence Through Aircraft Flow Fields and Wakes, AIAA 2001-2798

[10]   http://www.atmosculator.com/

[11]   L.C. Andrews, L.R. Phillips: Laser Beam Propagation through Random Media

[12]   D. Giggenbach, B.L. Wilkerson, H. Henniger, N. Perlot, Wavelength – Diversity   Transmission for Fading Mitigation in the Atmospheric Optical Communication Channel

[13]   Astronomy and Astrophysics 227, 294-300 (1990)

[14]   https://www.optics.arizona.edu

[15]   Wind Tunnel Validation of a CFD-Based Aero-Optics Model, AIAA 2007- 4011